Article type: Progress Report

Progress Report on Proton Conducting Solid Oxide Electrolysis Cells

*Libin Lei, Jihao Zhang, Zhihao Yuan, Jianping Liu, Meng Ni, Fanglin Chen**

Dr. L. Lei, Prof. J. Liu
Smart Energy Research Center, School of Materials and Energy
Guangdong University of Technology
Guangzhou 510006, PR China
Email: libinlei23@163.com

Dr. L. Lei, Dr. J. Zhang, Pro F. Chen
Department of Mechanical Engineering
University of South Carolina
Columbia, SC 29208, USA
Email: chenfa@cec.sc.edu

Dr. J. Zhang
State Key Laboratory of Power Systems, Department of Thermal Engineering
Tsinghua University, Beijing, PR China

Pro. Z. Yuan
School of Materials Science and Engineering,
Tianjin University of Technology
Tianjin 300384, PR China

Pro. M. Ni
Department of Building and Real Estate
The Hong Kong Polytechnic University
Hung Hom, Kowloon, Hong Kong, PR China

Keywords: solid oxide electrolysis cells, proton conductor, materials, modeling, current leakage

Abstract: Proton-conducting solid oxide electrolysis cell (H-SOEC) is a promising device that converts electrical energy to chemical energy. H-SOECs have been actively studied in the past few years, due to their advantages over oxygen-ion-conducting solid oxide electrolysis cells (O-SOECs), such as lower operation temperature, relatively lower activation energy, and easier gas separation. We present a critical overview of recent progress in H-SOECs, especially from 2014-2018. This review focuses on three aspects of H-SOECs, namely the materials, modeling and current leakage in proton conducting oxide electrolytes. Specifically, the current leakage in proton conducting oxides, which is often neglected, leads to two problems in the studies of H-

SOECs. One is the distortion of the electrochemical impedance spectra (EIS) and the other is low faradaic efficiency of electrolysis. Based on the comprehensive and critical discussion in these three sections, challenges in the development of H-SOECs are highlighted and prospective research in H-SOECs is outlined.

1. Introduction

Rapid growth in the world's population and economy, coupled with fast-paced urbanisation, has led to substantial demand in energy consumption and unanticipated adverse environmental impacts in the past several decades. Consequently, the need for clean, renewable and sustainable energy sources, such as solar, wind, hydro and tidal energy, has been growing significantly across the globe in recent years. However, due to site/location constraint and the intermittent nature of common renewable energy sources, reliable and affordable large-scale electricity storage is needed in order to secure a continuous and sustainable energy supply to meet the market's requirement [1]. Compared with battery systems, such as lead-acid battery and lithium-ion battery, converting electricity to fuel (such as hydrogen), through electrolysis, is more economical for large-scale electricity storage [2]. Among different types of electrolysis devices, solid oxide electrolysis cells (SOECs) operating at elevated temperatures have drawn considerable attentions [3]. Compared with electrolysis cells operated at low temperatures (room temperature to 473 K), SOECs offer a number of advantages due to the high operational temperature (773 K to 1273 K). One merit is that, according to the thermodynamics, electrolysis at high temperatures can substantially reduce the consumption of electric energy, which is compensated by heat energy. Since electric energy is more valuable than heat energy in general, electrolysis at high temperatures is more economical. Another benefit of high temperature electrolysis is that noble metal catalysts can be replaced with low cost materials with similar electrochemical

performance. Furthermore, only SOECs are regarded as capable of CO_2 electrolysis and co-electrolysis of CO_2-H_2O, which is a promising approach for the production of syngas and CO_2 utilization [3-4].

Depending on to the types of electrolyte, SOECs can be classified as, namely oxygen ion conducting SOECs (O-SOECs) and proton conducting SOECs (H-SOECs). To date, researches on SOECs are mainly focused on O-SOECs, in which oxygen ion is the charge carrier in the electrolyte. Some novel electrode materials, with good performance and durability, have been developed for O-SOECs [5]. Models, in different levels and operational conditions, have also been developed to study O-SOECs [6]. Moreover, some large-scale O-SOEC stacks and systems have been fabricated and tested [7].

Compared with O-SOECs, H-SOECs are significantly less prevalent in the literature and the development of H-SOECs is still at the early stage. H-SOECs have gradually garnered research attention in recent years, largely because H-SOECs possess some unique merits over O-SOECs, such as potentially lower operation temperature (773 K-973 K), relatively low activation energy, and ease in gas separation. The comparison between O-SOEC and H-SOEC is discussed in detail in the following section.

1.1 Comparison between O-SOEC and H-SOEC

Figure 1 shows the schematics of O-SOEC and H-SOEC. Compared with O-SOEC, the most distinct difference of H-SOEC is that the electrolyte is proton conducting instead of oxygen-ion conducting, resulting in different working principle. When an external voltage is applied to H-SOECs, protons are transported from the air electrode side to the fuel electrode side where hydrogen is generated. By contrast, the charge carrier in the electrolyte of O-SOECs is oxygen ion. The oxygen ions migrate from fuel electrode side to air electrode side when external voltage is applied. Steam is fed to the fuel electrode in O-SOECs, but to the air electrode in H-SOECs. Therefore, in

O-SOECs, to obtain dry hydrogen, the produced H_2 in the fuel electrode side needs an additional drying process. In contrast, in H-SOECs, dry and pure H_2 can be produced directly in the fuel electrode side, which can simplify the system and reduce the cost of operation. Furthermore, compressed hydrogen can be directly produced through increasing the operating pressure in the fuel electrode side (electrochemical compression). The in-situ utilization of the electrochemical compression can potentially increase the total energy efficiency and simplify the system, compared with external compression [8].

Besides ease in gas separation, H-SOECs can offer other advantages over O-SOECs. One noticeable merit is that the operation temperature of H-SOECs can be lower than O-SOECs, owing to the high ion conductivity and lower activation energy of proton conductors at relatively low temperatures (673 K to 973 K) [9]. The conventional O-SOECs are usually operated at high temperatures (between 973 K to 1273 K) due to the insufficient ionic conductivity of the electrolyte material at low temperatures [3]. High operation temperature leads to high cost in interconnect and sealing material. Therefore, when the operating temperature is reduced below 973 K, low-cost materials for balance-of-plant and interconnects could be used, resulting in cost reduction of the H-SOEC system [10]. Moreover, it can be predicted by thermodynamics that lowering the operation temperature can shift the composition of H_2O-CO_2 co-electrolysis product (H_2-CO) to CH_4. Compared with hydrogen, a product containing a high percentage of CH_4 has higher volumetric energy storage density [2].

Furthermore, it should mention that owing to their low operating temperatures and different working mechanisms, the durability of H-SOECs is expected to be superior to that of O-SOECs. It has been well known that lowering the temperature can mitigate the material degradation caused by corrosion or contamination [11]. For example, air electrode often suffers from Cr-poisoning due to the use of chromia forming alloy interconnect. The evaporation of Cr

species and the reactions between Cr species and air electrode materials can be greatly alleviated by lowering the operation temperature [12]. Furthermore, in O-SOECs, the Ni-based fuel electrode tends to be partially oxidized in an atmosphere with high humidity, leading to degradation of cell performance [13]. It has also been observed that the air electrode delaminates at high electrolysis current density due to elevated oxygen pressures at the electrolyte/air electrode interface [14]. By contrast, in H-SOECs, since the high sintering temperature during fabrication, the interface/adhesion between the fuel electrode and electrolyte layer is relatively strong and hydrogen is produced in the triple phase boundaries (TPBs) of fuel electrode, which is helpful to mitigate the problem of electrolyte/electrode delamination.

1.2 Brief History

This section briefly overviews the history of H-SOECs. Some milestones of the development of H-SOECs are highlighted and discussed. The first study concerning H-SOECs was reported in the early 1980s. Iwahara *et al.*[15] have experimentally demonstrated the proton conduction in $SrCeO_3$-based oxides by measuring the voltage of gas cells and then fabricated electrolyte-supported H-SOECs with $SrCe_{0.95}Sc_{0.05}O_3$ or $SrCe_{0.90}Sc_{0.10}O_3$ electrolyte layer (0.5 mm in thickness) and platinum (Pt) as symmetrical electrodes. By measuring the hydrogen evolution rate, the faradaic efficiency of electrolysis has been demonstrated to be 50-95% in the electrolysis current range of 0.1-0.8 A cm^{-2} at 1173 K. Beside Sc doping, Y or Yb doped $SrCeO_3$-based proton-conducting oxides have also been applied as the electrolyte materials of H-SOECs, showing similar electrolysis behavior [16]. It has been also found by Iwahara *et al.* that the faradic efficiency of electrolysis diminishes with increasing operating temperature and partial pressure of oxygen in the air electrode side, probably due to the increase in electronic conductivity in the electrolyte [16-17].

In 2008, Stuart *et al.* [18] reported that compared with $BaZr_{0.90}Y_{0.10}O_3$, $BaCe_{0.90}Y_{0.10}O_3$ is a better choice as the electrolyte material of H-SOECs due to its

higher protonic conductivity. However, the stability of $BaCe_{0.90}Y_{0.10}O_3$ in a H_2O-containing atmosphere has not been considered. In 2009, it was reported by Sakai *et al.* [19] that Pt electrodes showed poor activity in the air electrode as well as fuel electrode of H-SOECs. By contrast, the application of $Sr_{0.5}Sm_{0.5}CoO_3$ (SSC) in the air electrode and Ni in fuel electrode can significantly reduce the electrode overpotentials, resulting in much enhanced performance of H-SOECs.

Prior to 2010, all the studies about H-SOECs were conducted on electrolyte-supported cells, leading to large ohmic resistance from the electrolyte layer. The high ohmic resistance from the thick electrolyte layer limits the performance of H-SOECs, which hinders the development and practical application of H-SOECs. In 2010, for the first time, He *et al.* [20] reported the fabrication of Ni-$BaCe_{0.50}Zr_{0.3}Y_{0.20}O_3$ (BCZY53) fuel electrode supported H-SOECs with BCZY53 thin electrolyte layer and SSC-BCZY air electrode. H-SOECs with thin electrolyte layer show better electrochemical performance than those with thick electrolyte layer.

Figure 2 shows the number of SCI papers published for H-SOECs from 2008 to 2018. It is apparent that the researches of H-SOECs were relatively few prior to 2014, suggesting that H-SOECs did not receive too much attention. However, in the past two years (2017 and 2018), the number of SCI papers about H-SOECs increased greatly, especially in 2018, indicating that H-SOECs have garnered more and more research attention and funding support. It is important to note that in the past two years, there have been some breakthrough studies, which will be discussed in the following sections.

In 2014, Bi *et al.* [1] have timely summarized the past work progress of H-SOECs and highlighted the problems which have hindered the H-SOEC development. However, that review article is focused exclusively on experimental studies and modeling studies are not considered. Since 2014, much effort has been devoted to H-SOECs, resulting in some breakthrough studies with many more published papers. However, to date, there

has not been a comprehensive and critical review to summarize the recent progress of H-SOECs, especially the modeling studies, which is significant for the future study of H-SOECs.

Therefore, the aim of this progress report is to highlight the recent progress, especially from 2014-2018, in H-SOECs related to material's development and modeling studies. Some technical problems, such as the performance of the air electrodes and the current leakage in proton conducting electrolytes, are discussed in detail in this report. Finally, perspectives for the research and development of H-SOECs are provided.

2. Materials of H-SOECs

2.1 Electrolyte materials

As the electrolyte materials of H-SOECs, they have to fulfil several requirements. Possessing reasonable protonic conductivity and negligible electronic conductivity at the operating conditions is the basic requirement for the electrolyte materials. Furthermore, since the electrolyte layer is simultaneously exposed to a reducing atmosphere (fuel electrode side) and an oxidizing atmosphere containing high humidity (air electrode side), the electrolyte materials are required to maintain chemically stability in the dual atmospheric conditions. In addition, the electrolyte materials should also be chemically and physically compatible with common electrode materials such as Ni-cermet fuel electrodes and perovskite-type ceramic air electrodes.

To date, the most widely studied electrolyte materials for H-SOECs are ABO_3 (A=Ba, Sr, Ca; B=Ce, Zr) perovskite-type oxides [1, 3, 21]. As aforementioned, Iwahara *et al.*[15-16] have used Sc, Y or Yb doped $SrCeO_3$-based proton-conducting oxides as the electrolyte materials for H-SOECs. Since it has been experimentally and theoretically demonstrated that compared with $Sr/CaCeO_3$ and $Sr/CaZrO_3$-based oxides, $BaCeO_3$ and $BaZrO_3$-based oxides show better hydration capability and higher protonic conductivity [21-22], the latter have been extensively utilized as proton-conducting oxides in the past

decades [23]. However, neither $BaCeO_3$ nor $BaZrO_3$-based oxides can meet all the requirements as electrolyte for H-SOECs. Although $BaCeO_3$-based oxides possess superior protonic conductivity and good sinterability, it has been thermodynamically[24] and experimentally[25] demonstrated that $BaCeO_3$-based oxides are chemically unstable in a H_2O-containing atmosphere at typical operating conditions of H-SOECs. Although $BaZrO_3$-based oxides have been demonstrated to be chemically stable in a H_2O-containing atmosphere [26], the high resistance of grain boundary and refractory nature place significant challenges for the application of $BaZrO_3$-based oxides as electrolyte materials for H-SOECs [27].

2.1.1 $BaCe_{1-x}Zr_xO_3$-based materials

Therefore, to meet all the requirements, the most common strategies adopted by various researchers are to form $BaCe_{1-x}Zr_xO_3$-based solid solution [28], as shown in **Table 1**. Huan *et al.* [29] have fabricated H-SOECs with $BaCe_{0.5}Zr_{0.3}Y_{0.2}O_{3-\delta}$ (BCZY53) electrolyte layer and the electrolysis cells show relatively stable performance in short-term (30 h) testing. Although partial substitution of Ce by Zr in $BaCeO_3$-based oxides can improve the H_2O-tolerance of material, it has been reported that this approach can't completely stabilize the $BaCeO_3$-based oxides in an atmosphere containing high humidity [30]. Hakim *et al.* [30] have observed $Ba(OH)_2{\cdot}8H_2O$ on the BCZY53 electrolyte after 110 h operation and the formation of $Ba(OH)_2{\cdot}8H_2O$ is due to the reaction between BCZY53 and H_2O. Yang *et al.* [31] have also reported that $BaCO_3$ and CeO_2 can be found in $BaCe_{0.8-x}Zr_{0.2}In_xO_{3-\delta}$ (x=0, 0.1, 0.2, 0.3, 0.4) after exposure of the sample in moist air (20% H_2O) at 1023 K for 60 h.

To further improve the chemical stability of $BaCe_{1-x}Zr_xO_3$-based solid solution, other dopants such as Yb have been explored. Yang *et al.* [32] reported for the first time that Yb doping can greatly improve the stability of $BaCe_{1-x}Zr_xO_3$-based solid solution and $BaCe_{0.7}Zr_{0.1}Y_{0.1}Yb_{0.1}O_{3-\delta}$ (BCZYYb) is chemically stable after treatment in 50%H_2-50%H_2O or 50%H_2-50%CO_2 at 1023 K for 300 h. H-SOECs with BCZYYb electrolyte

have been successfully fabricated and tested. There is no observable degradation during the electrolysis test in 10~20%H_2O-air for less than 80 h [33]. Recently, Duan *et al.*[34] have tested BCZYYb-based H-SOECs (10%H_2O-air in the air electrode) for 1200 h at 823 K and the degradation rate is less than 30 mV per 1000 h. However, in some harsh conditions (with concentrated H_2O and CO_2), decomposition of BCZYYb can still be found in short-term (100 h) testing [35], suggesting that even Yb doping is not able to completely stabilize $BaCe_{1-x}Zr_xO_3$-based solid solution. Consequently, the chemical stability of $BaCe_{1-x}Zr_xO_3$-based solid solution is still a serious concern for the long term operation for H-SOECs. To prevent the BCZYYb electrolyte layer from the direct exposure to the steam, $La_2Ce_2O_7$ (LCO) has been applied as a protective layer in the air electrode side. However, the introduction of LCO protective layer leads to decrease of open circuit voltage, electrochemical performance of H-SOECs and faradaic efficiency of electrolysis, which may be due to the relatively lower ionic transport number of LCO and the mild reaction between LCO and the air electrode material ($Pr_2NiO_{4+\delta}$,PNO) [36].

2.1.2 $BaZrO_3$-based materials

Unlike $BaCe_{1-x}Zr_xO_3$-based solid solution, $BaZrO_3$-based oxides have been proven to be chemically stable in an atmosphere containing high concentration of H_2O and CO_2 [35a, 37], making them the ideal candidate of durable electrolyte materials of H-SOECs. Unfortunately, to use $BaZrO_3$-based oxides, a number of technical challenges such as high grain boundary resistance and poor sinterability have to be addressed. To achieve dense samples and reduce the grain boundary resistance, various methods have been investigated. One efficient way is adding sintering aids such as NiO, CuO, Li_2O and ZnO [38]. It has been reported by Tao et al. [38c] that 1 wt.% ZnO addition can significantly improve the sinterability of $BaZr_{0.8}Y_{0.2}O_{3-\delta}$ (BZY20). However, it has recently been discovered that adding NiO, CuO or ZnO into BZY20 has a negative effect on the proton conductivity and promotes the hole conduction in an oxidizing atmosphere [39]. The

increase of hole conduction (electronic conductivity) is detrimental for their application as electrolyte in H-SOECs, which requires electronic conductivity as low as possible.

Yttrium (Y) is the most studied doping element for $BaZrO_3$-based oxides, due to the high proton conductivity of BZY. To further improve the sinterability and proton conductivity of $BaZrO_3$-based oxides, co-doping of Y and other elements, such as Yb, Nd, Pr, In and Sn, have been investigated and some promising results have been achieved [40]. However, the effect of co-doping on the electronic conductivity or transport number of electron hole in the co-doped BZY electrolyte and needs to be evaluated in further studies.

Besides adding sintering aid and co-doping, alternative fabrication process has also been explored to improve the sinterability of $BaZrO_3$-based oxides. Pulsed laser deposition (PLD) has been applied to fabricate highly textured, epitaxially oriented BZY20 film, showing superior proton conductivity (0.11 S cm^{-1}) at 773 K [41]. However, PLD is an expensive process and is difficult for large-scale production of electrolyte for H-SOECs. In addition, some facile sintering methods have been developed to fabricate dense BZY films [27a, 42]. Bi *et al.* [42a] have fabricated dense BZY20 electrolyte layer by using a novel ionic diffusion strategy, taking the advantage of good sinterability of In-doping for $BaZrO_3$. Tong et al. [27a] have fabricated dense BZY20 samples with high conductivity by using solid-state reactive sintering, which is an easy and economic method. Recently, for the first time, microwave sintering technique has been adopted to fabricate $BaCe_{1-x}Zr_xO_3$-based electrolyte, showing high promise to reduce the sintering temperature to fabricate proton-conducting oxides with dense and uniform microstructures [43].

From **Table 1**, it can be seen that most of the studies on H-SOECs have been focused on using $BaCe_{1-x}Zr_xO_3$-based solid solution as electrolyte material while $BaZrO_3$-based H-SOECs have been reported in very few studies, probably due to the

relatively low conductivity and poor sinterability of $BaZrO_3$-based oxides. The first work on H-SOECs with $BaZrO_3$-based thin electrolyte has been performed by Bi *et al.*[26], using ionic diffusion method to fabricate $BaZrO_3$-based dense electrolyte. H-SOECs with thin and dense BZY20 thin electrolyte have also been successfully prepared by drop-coating method with 1.0 wt.% NiO as a sintering aid [44]. Shi *et al.* [45] have also fabricated BZY20-based H-SOECs for H_2O electrolysis and CO_2 conversion simultaneously. Similar to $BaZrO_3$-based oxides, $CaZrO_3$-based oxides also show high chemical stability in a humidified atmosphere and $CaZr_{0.9}In_{0.1}O_{3-\delta}$ (CZI) has been studied as electrolyte material of H-SOECs [46]. However, the application of $CaZrO_3$-based oxides as electrolyte materials is hindered by their low proton conductivity at low temperatures. Although, $BaZrO_3$-based H-SOECs haven't shown the performance comparable to those with $BaCe_{1-x}Zr_xO_3$-based electrolyte, there is still enormous potential for the development of $BaZrO_3$-based H-SOECs, thanks to their excellent chemical stability and high bulk proton conductivity.

2.1.3 Other materials and challenges

There are other proton-conducting oxides, such as $LaMeO_3$ (Me=Sc, In, Y…), $Ba_2In_2O_5$, $La_2Ce_2O_7$, $LaNbO_4$, La_6WO_{12}, highly doped CeO_2, $Ca_{12}Al_{14}O_{33}$ and $La_2Zr_2O_7$. However, due to various issues such as poor stability, low protonic conductivity and high electronic conductivity, these materials haven't been widely used as electrolyte materials for H-SOCs [47]. Further optimization of these materials will be needed for their application.

It is worth mentioning that Cr-poisoning is an issue of the stability of electrolyte materials. Chromia-forming alloys are the desirable choice of interconnects for H-SOECs at intermediate temperatures, due to their low cost, good conductivity and mechanical strength. However, volatile gaseous Cr species from the Cr-containing alloys result in Cr poisoning of the electrolyte/air electrode and performance degradation in solid oxide cells (SOC) [11]. According

to thermodynamics calculations, the partial pressure of volatile Cr species ($CrO_2(OH)_2$) in wet atmospheres is much higher than that in dry atmospheres (CrO_3) [12]. In addition, it has been demonstrated that higher humidity leads to faster evaporation of Cr from the Cr-containing metallic interconnect [48] and the deposition rate of Cr on the components of SOCs is proportional to the partial pressure of volatile Cr species [49]. Therefore, both in term of thermodynamics and kinetics, high humidity in the air electrode side of H-SOECs can aggravate Cr poisoning. However, until now, there is scarce study of Cr poisoning, even in H-SOFCs. Zhao et al. [50] have found that BCZY71 reacts with Cr_2O_3 to form $BaCrO_4$ even at 873 K under atmospheric environment, leading to a decrease of conductivity. It can be reasonably predicted that the Cr contamination on the electrolyte materials would be more serious in H-SOECs, due to the high concentration of steam in the air electrode side. Therefore, the Cr-poisoning problem in H-SOECs deserves further study.

The evaporation rate of Cr is directly related to the oxidation and corrosion behavior of metallic interconnect (typically chromia-forming alloy), because the oxidation and corrosion stability of metallic interconnect depends on the formation of a passivating chromium oxide layer on the surface. Zhao *et al.* [51] have found that the effect of water content in the air on the oxidation rate is different between alloy 430 and 411, which may be due to the differences in the alloy composition and alloy grain size. It has been reported that sever corrosion has been observed for ferritic steel AISI441 when exposed to dual atmosphere conditions with humid hydrogen on one side and humid air on the other. However, only thin protective chromia scales will be formed for such samples when exposed in only single atmosphere [52]. Therefore, the corrosion and oxidation behavior of stainless-steel metallic interconnect under the typical operation condition of H-SOECs deserves further study.

2.2 Air electrode materials

The air electrode has a paramount effect on the durability and performance of H-SOECs. The air electrode materials need to be chemically stable under moist air during

operation. They should also be chemically and physically compatible with the common proton-conducting electrolyte materials. Moreover, to achieve good performance and minimize polarization resistances, the air electrode materials should possess sufficient electronic conductivity, ionic conductivity as well as good catalytic activity for H_2O oxidation.

In the initial studies, metal electrode such as Pt, was used as the air electrode material of H-SOECs [15a, 18]. However, analogous to the development of solid oxide fuel cells (SOFCs), Pt electrode has been abandoned due to its high cost and low performance in H-SOECs. In **Table 1**, it can be seen that the perovskite-structured materials are the common air electrode materials of H-SOECs, which is attributed to the fact that perovskite-related structure can provide desirable electronic and ionic conductivity and catalytic activity. In addition, perovskite-structured electrode materials are more likely to be chemically and physically compatible with $BaCeO_3$ and $BaZrO_3$-based oxides, which also possess perovskite structure. There are three main categories of perovskite-related oxides, namely cubic-type perovskites (ABO_3), double perovskites ($AA'B_2O_6$) and Ruddlesden-popper (R-P) structure ($A_{n+1}B_nO_{3n+1}$) [53]that have been applied as the air electrode materials in H-SOECs.

2.2.1 Stability

The basic requirement of air electrode materials is that they should be chemical stability in humid air, containing acidic gases (H_2O-CO_2). Cubic-type perovskites (ABO_3) and double perovskites ($AA'B_2O_6$) usually contain alkaline earth elements, such as Sr and Ba, since the alkaline earth elements have the ionic size and valence favorable for the A-site [54]. However, the basic nature of alkaline earth elements makes them thermodynamically favorable to react with acidic gases (H_2O-CO_2), leading to degradation in performance. $La_{0.60}Sr_{0.40}Co_{0.20}Fe_{0.80}O_{3-\delta}$ (LSCF), which is a widely studied electrode material for SOFCs, has been applied as the air electrode material in H-SOECs [26, 28d]. However, it has been reported that in O_2-CO_2(2.83%)-H_2O(2.64%), LSCF suffers a serious degradation at 873 K, which is ascribed to the impeded

oxygen activation and oxygen surface diffusion by the formation of $SrCO_3$ on the surface [55]. Similarly, $Ba_{0.50}Sr_{0.50}Co_{0.80}Fe_{0.20}O_{3-\delta}$ (BSCF) decomposes after heat-treatment in 75%H_2O –air at 973 K, making it unsuitable as the air electrode material in H-SOECs [56]. One effective strategy to improve the stability of perovskite structure oxides in a humid atmosphere is to partially replace the alkaline earth elements by other elements with higher acidity, such as lanthanide elements. For example, to improve the stability of $Sr_3Fe_2O_{7-\delta}$ in high steam atmospheres, Huan *et al.*[29, 57] have developed $Sr_{2.8}La_{0.2}Fe_2O_{7-\delta}$ and $SrEu_2Fe_2O_{7-\delta}$ as robust air electrode materials for H-SOECs, by doping the A-site using La and Eu elements with high acidity. $Ln_{1.2}Sr_{0.8}NiO_{4+\delta}$ (Ln=La and Pr) have also been studied as the air electrode materials in H-SOECs, maintaining stable crystalline structure over 100 h in 20% $H_2$0-air at 1073 K [58]. Recently, Norby *et al.* [8] have investigated the chemical stability of mixed electronic and protonic conductors ($Ba_{1-x}Gd_{0.8}La_{0.2+x}Co_2O_{6-\delta}$, BGLC) in high steam pressures and found that when x=0.5, BGLC is chemically stable in 1.5 bar of steam for 100 h at 873 K, making it suitable as the air electrode material for H-SOECs.

Besides partially replacing alkaline earth elements, another feasible approach is to develop alkaline earth element-free air electrode materials, such as some R-P structured oxides [54]. The first study on H-SOECs with R-P structured air electrode ($La_2Ni_{0.6}Fe_{0.4}O_{3-\delta}$, LNF) has been reported by Lyagaeva *et al.,* where reasonable cell performance has been demonstrated both in fuel cell and electrolysis mode [59]. Lyagaeva *et al.* [60] have also applied another R-P structured oxide ($Nd_{1.95}Ba_{0.05}NiO_{4+\delta}$, NBN) as the air electrode material in H-SOECs. NBN exhibits good chemical stability coupled with electrochemical tolerance (no overpotential degradation) against highly moisturized atmospheres. $Pr_2NiO_{4+\delta}$ (PNO), possessing R-P structure and good catalytic activity, has been studied as the air electrode material in H-SOECs. Owing to the diffusion of Ba from BCZY to PNO, the structure of PNO changes from orthorhombic to tetragonal after high temperature treatment. Interestingly, such change of crystalline structure is not detrimental to the electrochemical performance [61].

Another potential concern of the stability of air electrode materials is chromium poisoning. As noted above, the high humidity in the air electrode side can aggravate the evaporation of Cr species, leading to more serious Cr contamination. However, until now, there haven't been any studies about Cr poisoning in the air electrode of H-SOECs. Therefore, with the development of H-SOECs, research attention should be given to this problem.

2.2.2 Electrochemical performence

The electrochemical performance of air electrode is the limiting factor of the cell performance of H-SOECs, especially at relatively low temperatures. Consequently, it is necessary to develop air electrode materials with good catalytic activity for H_2O oxidation and desirable electrical conductivity. In the early stage of the development of H-SOECs, researchers just directly used air electrode materials such as LSCF and SSC, which are commonly used in O-SOECs, without considering the uniqueness of the working principle in H-SOECs. As a result, these traditional air electrode materials show unsatisfactory electrochemical performance for H-SOECs.

Through analysis of the electrochemical impedance spectra (EIS) of H-SOCs, He *et al.* [20] have concluded that in H-SOECs, the rate-limiting steps for air electrode electrochemical process are the transfer of protons from decomposed water to the TPBs and the migration of protons from TPBs to the electrolyte, which is quite different from that of O-SOECs. Therefore, increasing the proton conductivity instead of oxygen-ion conductivity in the air electrode is crucial for improving the performance of H-SOECs. One frequently used method is to fabricate composite electrode by mechanically mixing proton-conducting phase (usually electrolyte material) with electron/oxygen-ion-conducting phase (electrode material) [26, 28b, 44]. In this case, the electrochemical reaction sites are located on the interface between proton-conducting phase and electron/oxygen-ion-conducting phase.

To further extend the electrochemical reaction sites to the entire surface of air electrode particles, triple-conducting materials, possessing proton, oxygen-ion and electron conductivity,

have been proposed and developed for H-SOECs. The working mechanisms of air electrodes with different design have been illustrated and compared in detail [1, 61]. Through the thermogravimetric and EIS analysis, Grimaud *et al.* [62] have found that PNO, an electron/oxygen ion mixed conductor, can absorb H_2O in a wet atmosphere and the absorbed H_2O inserts into the crystal structure to form protonic defect, resulting a triple mixed $H^+/O^{2-}/e^-$ conductor. Subsequently, Li *et al.* [61] have applied PNO as air electrode material for H-SOECs and the triple mixed $H^+/O^{2-}/e^-$ conductivity of PNO has been further demonstrated by measuring the water insertion-induced electrical conductivity variation. This hydration behavior has also been found in $BaCo_{0.4}Fe_{0.4}Zr_{0.1}Y_{0.1}O_{3-\delta}$ (BCFZY) by thermogravimetric analysis, suggesting the existence of proton conductivity. H-SOFCs and H-SOECs with BCFZY air electrode show excellent performance and the polarization resistance is only 0.13 Ω cm^2 at 873 K [34-35]. Strandbakke *et al.* [63] have investigated some double perovskite oxides as air electrode materials on BCZY27 electrolyte and found that among these materials, $BaGd_{0.8}La_{0.2}Co_2O_{3-\delta}$ (BGLC) exhibits the best performance, possibly due to its unique hydration behavior. However, thermogravimetric analysis shows that in BGLC, detectable protonation only takes place below 723 K. Moreover, the hydration behavior (proton uptake) of $(Ba,Sr,La)(Fe,Co,Zn,Y)O_{3-\delta}$ perovskite oxides has been investigated and compared. The proton uptake is found to be heavily depended on the basicity of the oxide ions and covalent character of bonds between B site's metal and oxygen. Partial substitution of Zn on the B-sites greatly enhances the proton uptake, while Co substitution shows the opposite effect. This systematic study provides guidelines for developing triple-conducting air electrode materials of H-SOCs [64].

Not only chemical composition but also microstructure has a significant effect on the electrochemical performance of air electrode. A self-architectured ultraporous 3D air electrode consisting of hollow $PrBa_{0.5}Sr_{0.5}Co_{2-x}Fe_xO_{5+\delta}$ (PBSCF) fibers has been fabricated and applied to H-SOECs. The microstructure of the whole cell is characterized by 3D X-ray microscope and SEM, as shown in **Figure 3**. The air electrode possesses textile-like structure and well

adheres to the electrolyte. The H-SOECs with this 3D air electrode show better electrolysis performance than those with conventional sponge-like structured electrode [33b]. This excellent electrolysis performance can be ascribed to the fact that the hollow-fiber structure can provide aligned pores for gas diffusion and continuous pathways for the migration of electrons and ions. Moreover, Choi *et al.* [65] have used pulsed laser deposition (PLD) to fabricate a thin dense layer of PBSCF between the porous PBSCF air electrode and the electrolyte. The introduction of dense PBSCF layer can significantly improve the contact and decrease ohmic resistance, resulting in the best electrolysis performance (2000 mA cm^{-2}, at 1.3 V and 873 K) among the reported studies in **Table 1**.

Finally, in solid oxide fuel cells (SOFCs), it has been demonstrated that the performance of air electrode can be significantly enhanced by surface modification. The introduced particles or film on the surface of the air electrode can provide extra electrochemical reaction sites and pathways for the transfer of electrons and ions [66]. Surface modification has been successfully applied to proton conducting SOFCs (H-SOFCs) for improving the performance of air electrodes [67]. However, to date, there have been very few reports[46] about the application of surface modification technology in H-SOECs. It is reasonable to expect that surface modification would be an efficient approach to improve the performance of air electrode in H-SOECs, especially at low operating temperatures.

2.3 Fuel electrode materials

The fuel electrode materials should possess adequate electronic, ionic conductivity as well as catalytic activity for hydrogen evolution. Moreover, the fuel electrode materials are required to be chemically stable in a reducing atmosphere. In general, metals can be used as the fuel electrode materials of H-SOECs. Pt was initially used as the fuel electrode in H-SOECs[15a], however, its high cost hinders its further application. To date, Ni is the most commonly used fuel electrode of H-SOECs because of its low cost and good catalytic activity. To extend the TPBs in the fuel electrode and mitigate the mismatch of thermal expansion coefficient between

the fuel electrode and electrolyte, the common practice is to mechanically mix the electron-conducting phase (Ni) with proton-conducting phase (normally electrolyte materials).

Recently, feasibility of metal-supported H-SOECs has been investigated. Compared with Ni-based fuel electrode supports, metal supports can provide better mechanical ruggedness and tolerance to very rapid thermal cycling and redox cycling [68]. Wang *et al.* [69] have applied co-sintering to fabricate the metal-supported H-SOECs and found some critical issues of fabrication, such as the chemical stability of electrolyte materials, the densification of electrolyte layer, the contamination of electrolyte with Si and Cr from the metal support and the evaporation of electrolyte constituents in a reducing atmosphere during co-sintering. Consequently, more work has to be performed to realize the benefit of metal-supported H-SOECs.

2.3.1 Sinterability

To fabricate a thin electrolyte layer, the fuel electrode is usually made as the thickest cell component, providing mechanical strength for the entire cell. The fuel electrode support and the thin electrolyte layer are often co-sintered at high temperature. Therefore, the fuel electrode support is required to have good sinterability, which is critical for the densification and conductivity of the electrolyte layer [70]. Bi *et al.* [70a] have fabricated NiO-BZY20 fuel electrode support with traditional mechanically mixed powders and wet-chemically synthesized composite powders respectively, and found that the latter, with better sinterability, can promote the densification of BZY20 electrolyte and lower the sintering temperature of the electrolyte layer to 1573 K. Leonard *et al.* [71] have compared the H-SOECs with Ni-BCZY45 and Ni-SCZY45 fuel electrode substrate and found that Ni-SCZY45, which possesses better sinterability, is more favourable for the densification of the electrolyte.

The morphology of the fuel electrode also influences the performance and sinterability of the electrode. Yang *et al.* [72] have systematically investigated the effect of the amount of pore former (carbon microspheres) on the shrinkage, the porosity, thermal expansion and

electrochemical performance of NiO-BCZY71 electrode support. The H-SOCs, with 30 wt.% pore former, show the best performance, due to proper porosity and TPBs in the fuel electrode.

2.3.2 CO_2 conversion in the fuel electrode

It is worth mentioning that to date, the studies concerning H-SOECs are mainly focused on H_2O electrolysis. However, co-electrolysis of H_2O and CO_2 can also be conducted in H-SOECs [3, 45, 73], in which CO_2 is electrochemically converted to CO by reaction with proton or chemically converted to CO by reverse water gas shift reaction ($CO_2+H_2=CO+H_2O$) in the fuel electrode. In the case of co-electrolysis, additional requirement for the fuel electrode is to maintain chemical stability in an atmosphere containing CO_2, CO and H_2O. The thermal stability of $BaCe_xZr_{0.8-x}Y_{0.2}O_{3-\delta}$ (x=0-0.4) has been investigated in a CO_2-containing atmosphere and it has been found that when x is larger than 0.2, reaction with CO_2 will take place and $BaCO_3$ can be detected at above 823 K [74]. Moreover, oxidation of Ni should also be paid attention during co-electrolysis.

Shi *et al.*[45] have demonstrated efficient and controllable co-electrolysis of H_2O and CO_2 in H-SOECs using BZY as electrolyte and BZY-Ni as fuel electrode. The possible mechanism of CO_2 conversion in H-SOECs is proposed, as shown in **Figure 4**. On the BZY surface, the absorbed CO_2 reacts with oxygen vacancy and proton to form bicarbonate species (HCO_3^-), which finally decomposes to CO and H_2O. For the formation of CH_4, CO is ready to absorb over nickel surface and then receives hydrogen atoms to form CH_4. Interestingly, compared with pure steam electrolysis, the introduction of CO_2 in the fuel electrode side can accelerate the electrode kinetics, which is probably attributed to facile absorption of CO_2 on BZY surface. Danilov *et al.* [73c] have also observed CO_2-promoted effect in $BaCe_{0.5}Zr_{0.3}Dy_{0.2}O_{3-\delta}$ (BCZD)-based H-SOECs and explained this effect by a hypothesis that higher concentration of H_2O, caused by the introduction of CO_2 and reverse water gas shift reaction, results in enhancement of proton conductivity and electrochemical performance in the fuel electrode. However, it is noted that the fuel electrode microstructure should be carefully designed and optimized since

gas diffusion in the fuel electrode becomes more complicated for co-electrolysis than for steam electrolysis.

Generally speaking, the Ni-based composite electrode can meet the requirements of fuel electrode of H-SOECs. To achieve better performance, the sinterability and microstructure of fuel electrode need further optimization. The stability of fuel electrode in a CO_2-containing atmosphere should be taken into consideration in the case of H_2O and CO_2 co-electrolysis. Compared with Ni-based fuel electrode supports, metal supports can provide some unique advantages, but the fabrication of metal supported H-SOECs is more challenging and the technical problems of fabrication need to be addressed.

3. Modeling of H-SOECs

Until now, the modeling studies about H-SOECs are very limited. Ni *et al.* [75] have developed the basic electrochemical model of H-SOECs for steam electrolysis, in which concentration overpotential, activation overpotential and ohmic overpotential are taken into consideration. It has been found that the fuel electrode supported configuration is the most efficient design for H-SOECs for steam electrolysis due to easy H_2 transport in the fuel electrode. For comparison, a thick air electrode can cause high concentration loss, due to slow diffusion of steam and O_2 in the air electrode. A performance analysis of H-SOECs for syngas production has also been conducted by setting up an electrochemical model. The operating conditions such as configuration, temperature, pressure, ratio of H_2O and CO_2, have been investigated [76]. An important assumption in the aforementioned studies is that the electrolyte material is a pure proton conductor. As a result, the open circuit voltage (OCV) is calculated by conventional Nernst equation (equation I) and the proton flux in the electrolyte is calculated by ohm's law (equation II):

$$E = E^{\theta} + \frac{RT}{2F} \ln \left(\frac{P_{H_2} P_{O_2}^{\frac{1}{2}}}{P_{H_2O}}\right) \quad \text{(I)}$$

$$J_{OH^{\cdot}} = \frac{\eta_{ohm}}{R_{ohm}} \quad \text{(II)}$$

where E^{θ} is the standard potential, R is the ideal gas constant, T is temperature, F is the Faraday constant, P_x is the partial pressure of X, $J_{OH^{\cdot}}$ is the proton flux in the electrolyte, η_{ohm} is the ohmic overpotential and R_{ohm} is the ohmic resistance of electrolyte. However, it has been demonstrated that the commonly used proton conducting electrolyte materials such as BCY and BZY, are mixed conductors rather than pure proton conductor, especially at high temperature and in an oxidizing atmosphere [77]. Even when the oxygen ionic conductivity of the proton conducting electrolyte is considered, the predicted cell performance is different from that of a cell with a pure proton conducting electrolyte. This is because the oxygen ionic conductivity not only affects the OCV of the cell, but also allows the production of steam in the fuel electrode (in an SOFC), affecting the gas transport processes in the porous electrodes [78]. Hence, it is improper to assume pure proton conduction and directly use equation I and equation II for mixed conductors.

In the cases of whole cells with mixed conductors as electrolyte materials, the OCV can be expressed by the following equation (equation III-a) [59, 79]:

$$E = t_o E_o + t_H E_H = t_o \frac{RT}{4F} \ln\left(\frac{P'_{O_2}}{P''_{O_2}}\right) + t_H \frac{RT}{2F} \ln\left(\frac{P''_{H_2}}{P'_{H_2}}\right) \quad \text{(III-a)}$$

where E_o and E_H are the thermodynamic OCV values of oxygen and hydrogen cells, P'_{O_2} and P'_{H_2} are the partial pressure of oxygen and hydrogen in the oxidizing atmosphere, P''_{O_2} and P''_{H_2} are the partial pressure of oxygen and hydrogen in the reducing atmosphere, t_o and t_H are the transport numbers of oxygen ion and proton in the electrolyte. Equation III-a can be presented in another form as:

$$E = t_i \frac{RT}{4F} \ln\left(\frac{P'_{O_2}}{P''_{O_2}}\right) + t_H \frac{RT}{2F} \ln\left(\frac{P''_{H_2O}}{P'_{H_2O}}\right) \quad \text{(III-b)}$$

where $t_i = t_o + t_H$ is the transport number of ions. If the conductivity of oxygen ion is insignificant, t_i can be approximately equal to t_H.

Moreover, it is noteworthy that the influence of electrode polarization on the OCVs should be considered. The mathematical relationship between electrode polarization resistance and OCVs has been deducted by Liu *et al.*[80]:

$$E = t_i\left(\frac{R_i+R_e}{R_p+R_i+R_e}\right)E_N \quad \text{(IV)}$$

where R_i and R_e are the average ionic and electronic resistances of the bulk electrolyte, respectively. R_p is the electrode polarization resistance. According to equation (IV), the increase of R_p would lead to loss of OCV.

To accurately describe the motion of charged species in mixed conductors, it is preferred to use Nernst-Planck equation, instead of ohm's law, as shown below [81]:

$$J_i = -D_i\frac{\partial C_i}{\partial x} - \frac{\sigma_i}{z_i q}\frac{\partial \phi(x)}{\partial x} \quad \text{(V)}$$

where D_i is the diffusivity, C_i is the concentration, σ_i is the conductivity, z_i is valence of charges, q is the elementary charge and ϕ is the electrostatic potential. The relation between diffusivity and conductivity can be described by Nernst-Einstein relation, as shown in equation V [82]:

$$D_i = \frac{k_B T}{(z_i q)^2 C_i}\sigma_i \quad \text{(VI)}$$

where k_B is the Boltzmann constant.

As shown in equation V and VI, the concentration of charged species is an important variable for the flux and conductivity of charged species. When a mixed conductor is in a homogenous atmosphere (without the influence of electrostatic potential), the concentrations of defects (charged species) can be determined by calculation of thermodynamic equilibrium, as shown in the following reactions and equations [83]:

$$\frac{1}{2}O_2 + V_o^{\cdot\cdot} \Leftrightarrow O_o + 2h^{\cdot} \quad (1)$$

$$K_O = \frac{[C_{O_o}][C_{h\cdot}]^2}{p_{O_2}^{1/2}[C_{V_{\ddot{o}}}]} \quad \text{(VII)}$$

$$O_o + H_2O + V_o^{\cdot\cdot} \Leftrightarrow 2OH_o^{\cdot} \quad (2)$$

$$K_W = \frac{[C_{OH^{\cdot}}]^2}{p_{H_2O}[C_{O_o}][C_{V_o^{\cdot\cdot}}]} \quad (VIII)$$

where K_O and K_W are the equilibrium constants. Combining the above equilibrium equations and the law of mass conservation, the concentrations of defects can be predicted as functions of equilibrium constants and partial pressures of gases, as shown in **Figure 5**. It can be observed that the transport property of a mixed conductor is very different in different conditions. When an electric field or a gradient in chemical potential exists, it leads to inhomogeneous distribution of defects. Liu [84] has developed general analytical solutions to predict the distribution of charged defects in mixed conductors under an electric field or a gradient in chemical potential. The derived analytical solutions can also be used to determine the transport properties of a mixed conductor from observed steady-state behavior of the mixed conductor under controlled condition.

To determine the equilibrium constants (thermodynamic properties) and the concentrations of charged defects for a specific mixed conductor, it is necessary to measure the actual conductivity of the mixed conductor and then fit the experimental data. Zhu *et al.*[85] have measured the conductivity of BZY20 and BCZYYb in different oxygen partial pressure, subsequently fitted the experimental data with/without considering the immobile polaron traps, and finally determined the thermodynamic properties of these two proton-conducting materials. In addition, the obtained thermodynamic and transport properties have been incorporated into the Nernst-Planck model to simulate the transport behavior (such as faradaic efficiency) of proton-conducting cells in the fuel cell and electrolysis mode, as presented in **Figure 6**. It is clear that the proton-conducting cells, with BZY and BCZYYb as electrolyte materials, show a similar trend of faradaic efficiency. As the oxygen partial pressure increases, the faradaic efficiency in both fuel cell and electrolysis cell modes generally decreases, which is due to the

increase of concentration of electron hole in the electrolyte (reaction 1). It is noteworthy that the faradaic efficiency increases with the absolute electrolysis current density.

Besides the Nernst-Planck equation, other equations and models have also been developed to simulate the motion of charged defects in the mixed conductors. Virkar [86] has used Goldman-Hodgkin-Katz-type equation and equivalent circuits to build a model for SOFCs with mixed conductors as electrolyte materials. The transport behavior of all charged defects across the air electrode/electrolyte and fuel electrode/electrolyte interfaces is incorporated into the analysis of this model. Virkar [87] has also used Onsager equations and equivalent circuits to describe the motion of charged defects in mixed conductors in the electrolysis mode. The Onsager equation can be written as:

$$J_i = \sum_k L_{ik} X_k \tag{IX}$$

where J_i is the thermodynamic flux, L_{ik} is the Onsager coefficient and X_k is the thermodynamic force.

Activation loss and concentration loss in the electrode also have significant effect on the performance of H-SOECs. Since the working principle of H-SOECs is different from O-SOECs or H-SOFCs, the equations for calculating overpotential of electrode in H-SOECs are unique. The activation overpotential of fuel electrode and air electrode can be expressed by the Butler-Volmer equation[81a, 88]:

$$\eta_{act,i} = \frac{RT}{F} \ln \left[\frac{|J_{H^+}|}{2J_{0,i}} + \sqrt{\left(\frac{|J_{H^+}|}{2J_{0,i}}\right)^2 + 1} \right] \tag{X}$$

where J_{H^+} is current density of proton, $J_{0,i}$ is exchange current density and i represents fuel electrode or air electrode.

The concentration overpotentials of H-SOECs can be expressed in terms of the gas concentration difference between the electrode surface and the electrode-electrolyte interface as follows:

$$\eta_{conc,fuel} = \frac{RT}{2F} \ln \left(\frac{P_{H2}^{I}}{P_{H2}^{0}}\right) \quad \text{(XI)}$$

$$\eta_{conc,air} = \frac{RT}{2F} \ln \left[\frac{(P_{O2}^{I})^{\frac{1}{2}} P_{H_2O}^{O}}{(P_{O2}^{O})^{\frac{1}{2}} P_{H_2O}^{I}}\right] \quad \text{(XII)}$$

where P_x^I represents concentration of x at the interface of electrode and electrolyte.

Despite of some preliminary modeling studies on H-SOEC at single cell level, no comprehensive thermo-electrochemical models have been reported on H-SOEC stacks. It is important to fully consider the electrochemical reactions, electronic/ionic transport, gas transport and heat transfer since all these processes are highly coupled. For example, due to the gas composition variation in an H-SOEC stack, the electrochemical reaction rates and thus the temperature distribution in the stack can be non-uniform. To predict and optimize the stack performance, higher level models are needed. In addition, there is a lack of detailed modeling studies on the H_2O/CO_2 co- electrolysis processes in an H-SOEC, which is very different from steam electrolysis. To facilitate H-SOEC design optimization, modeling studies at various levels for H-SOECs are needed.

4. Current leakage and Faraday efficiency of electrolysis

In the studies of H-SOECs, a critical issue which is often neglected is the current leakage in proton conducting oxides. The current leakage is caused by the non-negligible electronic conductivity, which is associated with the existence of electron holes. For instance: in an oxidizing atmosphere, the total transport number of ions (proton and oxygen ion) of BZY20 is only 0.52 and the transport number of electron hole reaches 0.48 at 873 K [77b]. The current leakage in proton conducting oxides leads to two problems in the electrochemical testing of H-SOECs. Firstly, the electrochemical impedance spectra (EIS) of symmetrical cells or whole cells can't reflect the real ohmic resistances and polarization resistances without proper corrections (distortion of impedance spectra). Secondly, the actual protonic current density in

the electrolyte is smaller than the detected external electrolysis current density in H-SOECs, leading to low faradaic efficiency of electrolysis.

4.1 Distortion of impedance spectra

The validity of EIS in proton conducting symmetrical cells has been questioned by Poetzsch *et al.* [89]. Through comparing the EIS of BSCF on yttria-stabilized zirconia (YSZ, pure oxygen ion conductor) and BZY15, it has been found that the polarization resistance of BSCF on BZY15 is smaller than that on YSZ by one order of magnitude. The unexpected small polarization resistance of BSCF on BZY15 can't be ascribed to the different reaction mechanism but the current leakage in BZY15. In other words, when the EIS of symmetrical cells with proton conducting oxides as electrolyte are measured, the apparent resistances of EIS aren't real and can't reflect the real electrode kinetics. Therefore, the electronic conductivity of the electrolyte should be taken into account for reliable analysis of EIS measured for samples with proton-conducting electrolyte.

The current leakage in proton conducting electrolyte takes place not only in symmetrical cells but also in whole cells. Hence, in the EIS of whole cells, the intrinsic ohmic resistance and polarization resistance are also concealed. To evaluate the intrinsic resistances of whole cells, Huan *et al.* [29] have developed a feasible method by building an equivalent circuit for EIS, in which electronic leakage is taken into consideration. The equivalent circuit and corresponding simulated EIS are shown in **Figure 7**. According to the equivalent circuit, the apparent ohmic resistance (R_s) can be calculated as functions of ionic resistance (R_i) and electronic resistance (R_e)[80]:

$$R_s = \frac{R_i R_e}{R_i + R_e} \quad \text{(XIII)}$$

The transport number of ions (t_i) can be determined by using the equation below:

$$t_i = \frac{R_e}{R_i + R_e} \quad \text{(XIV)}$$

The total apparent resistance (R_T) can be derived by using the following equation:

$$R_T = \frac{(R_i+R_{p,r})R_e}{(R_i+R_{p,r})+R_e} \quad \text{(XV)}$$

The calculation formula for real polarization resistance is shown below:

$$R_{p,r} = \frac{(R_T-R_S)R_S}{t_i[t_iR_T-(R_T-R_S)]} \quad \text{(XVI)}$$

From equation XVI, it can be easily derived that when t_i=1, $R_{p,r}$ is equal to (R_T-R_s), meaning that $R_{p,r}$ and R_p are identical. While t_i<1 (not pure ion conductor), $\frac{R_{p,r}}{R_p} = \frac{R_S}{t_i[t_iR_T-(R_T-R_S)]} > 1$, indicating that the real polarization resistance ($R_{p,r}$) is larger than the apparent polarization resistance (R_p). Consequently, when the electrolyte material is a mixed conductor with non-negligible current leakage, the result of EIS should be corrected for the analysis of real resistances, performance and electrode kinetics.

4.2 Faraday efficiency of electrolysis

The other problem caused by the existence of current leakage is deviation of faradaic efficiency of electrolysis from the theoretical one. Iwahara *et al.* [15a] have reported that in the electrolyte-supported H-SOECs, the faradaic efficiency for hydrogen evolution ranges from 50%-95%. Babiniec *et al.* [90] have fabricated H-SOCs with thin BCZY27 electrolyte layer and Ni-BCZY27 fuel electrode support, and measured the current efficiency in galvanic operation (fuel cell mode) and electrolytic operation (electrolysis mode). In the electrolytic operation, the faradaic efficiency is only 32% at 100 mA and 973 K. It has also been reported that in the fuel electrode supported H-SOECs with BZY20 as electrolyte material, the faradaic efficiency of electrolysis is about 64% at 1.3 V and 873 K [44]. According to the above experimental observation, the detected external electrolysis current doesn't reflect the real hydrogen evolution rate and the faradaic efficiency of electrolysis in H-SOECs can not reach 100%. However, in some studies of H-SOECs, this problem has been neglected by highlighting "high" electrolysis current density without measuring the actual hydrogen evolution rate.

The low faradaic efficiency of electrolysis is detrimental to the overall energy efficiency of H-SOECs, hence it is necessary to study its influential factors and increase the faradaic efficiency. The most direct approach to increase faradaic efficiency is to suppress the electronic conductivity in the electrolyte materials. For BZY, BCZY or BCY, it has been experimentally and theoretically demonstrated that the electronic conductivity is highly related to operating temperature and decreases considerably with lowering the temperature [77, 91]. Therefore, reducing the operation temperature of H-SOECs is a feasible method to increase the faradaic efficiency of electrolysis. It has been reported that the faradaic efficiency of electrolysis can reach 99.6% at 1.2 V and 773 K in H-SOECs with BCZYYb as electrolyte material [33b]. However, at such a low temperature, the large resistance from the electrolyte and electrode is a challenge. In addition, the partial pressures of O_2 and H_2O are also the influential factors of electronic conductivity. **Figure 8** shows the partial conductivity of oxygen ion, proton and electron hole in BCZY27 as a function of pH_2O [91]. It is obvious that at 1073 K and 873 K, the electronic conductivity at pO_2=0.2 atm is larger than that at $pO_2=10^{-5}$ atm, meaning that higher partial pressure of O_2 leads to larger electronic conductivity. The influence of pO_2 on electronic conductivity can be explained by the thermodynamic equilibrium of reaction 1, in which higher partial pressure of O_2 is thermodynamically favorable for the formation of more electron holes. In all four cases (**Figure 8 (a)-(d)**), the electronic conductivity diminishes gradually with the increase of pH_2O, while the proton conductivity shows the opposite trend, which is due to the fact that increasing pH_2O is thermodynamically favorable for the formation of proton defect (reaction 2) and can suppress the formation of electron hole.

Besides temperature and gas composition, the chemical composition of the proton conducting oxides also dictates the electronic conductivity/transport number of electron hole. Han *et al.* [92] have systematically investigated the influential factors of transport numbers in $BaZrO_3$. Through comparing different doping elements (Y, In, Ho, Er, Tm and Yb), it has been found that doping Y to $BaZrO_3$ results in the smallest transport number of electron hole. In

addition, the transport number of electron hole decreases with the content of Y doping from 10 to 20 mol%, but does not further decrease when the Y content is larger than 20 mol%. Furthermore, both Ba-deficiency and Ba-excess lead to an increase in the transport number of electron hole. Han *et al.* [39] have also evaluated the effect of sintering additive (NiO, CuO and ZnO) on the transport properties of BZY20 and the experimental results show that addition of sintering additives leads to an increase of the transport number of electron hole. Such enhancement in contribution of hole conduction might correlate with the decreased capability for hydration. Dippon *et al.* [93] have investigated the influence of the cerium content in the BCZY membranes on the magnitude of the current leakage. The feeding of dry He-Ar in the Au electrode can minimize the proton and oxygen ion conductivity in the membrane, leading to a fact that electron holes are the main charge carriers under this testing conduction. As presented in **Figure 9**, compared with BCZY18 and BZY10, the responding current density of BCZY27 is much larger, suggesting that the current leakage is more serious in BCZY27 and the content of cerium has significant effect on the electronic conductivity of BCZY. Moreover, it has been found that partial substitution of Ba by Ca or Sr can increase the proton concentration and hence the total ion transfer number [94]. However, there have been very limited studies concerning the influence of chemical composition on the electronic conductivity (transport number of electron hole) of proton conducting oxides, especially for the application of H-SOECs. In the future, more efforts should be devoted to optimize the chemical composition of proton conducting oxides for H-SOECs.

Inspired by the application of electronic-blocking layer in oxygen-ion conducting SOFCs [95], adding an electronic-blocking layer in H-SOECs seems to be a feasible solution to suppress the current leakage in the electrolyte layer. However, to date, there are limited studies about the electronic-blocking layer in H-SOECs or H-SOFCs. Peng *et al.* have reported the in-situ formation of electron-blocking layer ($Ba(Ce,Zr)_{1-x}(La,Dy,In)_xO_{3-\delta}$) for H-SOFCs with proton conducting electrolyte ($La_{1.9}In_{0.1}Ce_2O_7$) and Ni- $BaCe_{0.5}Zr_{0.3}Dy_{0.2}O_{3-\delta}$ fuel electrode [96]. The

prerequisite of material using for the electron-blocking layer in H-SOECs or H-SOFCs is that it should possess high proton transference number and good stability in a reducing or oxidizing atmosphere.

As stated previously, in general, lowering the operation temperature, reducing the partial pressure of oxygen, increasing the partial pressure of steam and adding an electronic-blocking layer are feasible approaches to suppress the electronic conductivity of proton conductors, which is beneficial for increasing faradaic efficiency of H-SOECs. Meanwhile, rationally controlling the chemical composition of proton conducting electrolyte is also important to improve faradaic efficiency.

Finally, the external current (externally applied voltage) plays an important role on the faradaic efficiency of electrolysis. As shown in **Figure 10** [97], at 973 K and 873 K, the deviation of actual hydrogen evolution rate from the theoretical one (faradaic efficiency=100%) increases with the electrolysis current density, indicating that faradaic efficiency of electrolysis drops with the increase of external current (externally applied voltage). A similar trend of faradaic efficiency has also been found in H-SOECs with BCZYYb, BCZY71, BCZY53 or BCZY27 as electrolyte materials [29, 33b, 57, 90]. However, opposite trend of faradaic efficiency has been experimentally observed by Duan *et al.*[34] and theoretically simulated by Zhu *et al.* [85] (**Figure 6**) in H-SOECs with BZY and BCZYYb as electrolyte materials. The discrepancy from different studies suggests that there is a knowledge gap about the true influence of external applied voltage on the faradic efficiency of H-SOECs. More efforts will be critically needed to study this problem.

5. Summary and Outlook

H-SOECs have gradually attracted research attentions in the past decade due to some unique advantages over O-SOECs. Recent progress (from 2014-2018) of H-SOECs in terms of materials and modeling is highlighted and discussed. Most of the efforts in H-SOECs have so far focused on the electrolyte materials and air electrode

materials. For electrolyte materials, $BaCe_{1-x}Zr_xO_3$-based solid solutions, possessing reasonable conductivity and acceptable chemical stability, are the most used materials in H-SOECs. Furthermore, if the problems of poor sinterability and large resistance of grain boundary can be properly addressed, $BaZrO_3$-based oxides would become desirable electrolyte materials for H-SOECs. In term of air electrode, maintaining chemical stability in a H_2O and CO_2-containing atmosphere is the essential requirement. Because of the acidic nature of H_2O and CO_2, it is preferred to decrease the content of elements with high basicity (such as alkaline earth elements) in the air electrode materials. The electrochemical performance of air electrode is a limiting factor to the overall performance of H-SOECs, especially at relatively low operating temperatures. Using the triple-conducting materials and optimizing the microstructure have been demonstrated to effectively enhance the performance of air electrode in H-SOECs. It is noteworthy to mention that Cr-poisoning could be a serious issue in H-SOECs, however, very limited effort has been devoted to this topic yet.

To date, the researches concerning modeling of H-SOECs are still very limited. In the initial stage, based on an assumption that the electrolyte materials are pure proton conductors, some models have been developed to simulate the electrochemical performance of H-SOECs. However, the effect of electronic conductivity in proton conducting electrolyte can't be neglected. Therefore, to build a precise electrochemical model to describe H-SOECs, the electronic conductivity should be taken into account. Combining equivalent circuits with the Nernst-Planck equation, Goldman-Hodgkin-Katz-type equation or Onsager equation may be feasible to simulate the transport behavior of proton/electron mixed conductor. In addition, only single cell level models have been reported on H-SOECs and there is a lack of comprehensive 3D thermo-electrochemical modeling to fully consider the electrochemical reactions, electronic/ionic transport, gas transport and heat transport in H-SOEC stacks, which is

vitally needed for stack performance prediction and optimization. In the future, the simulation of H-SOECs will need more effort.

Current leakage is a critical issue in proton conducting oxides, but this hasn't received adequate attention in H-SOECs, leading to unreliable analysis of experimental results. Because of current leakage, EIS may not reflect the intrinsic ohmic resistance and polarization resistance without proper correction and the actual faradaic efficiency of electrolysis may be significantly deviated from the mere calculation of the electrolysis current. Therefore, to conduct a reliable analysis of H-SOECs, the EIS has to be corrected and the actual evolution rate of hydrogen production must be measured in H-SOECs. Suppressing the current leakage is beneficial to the improvement of energy efficiency of H-SOECs. Lowering the operation temperature, reducing the partial pressure of oxygen, increasing the partial pressure of steam and adding an electronic -blocking layer are effective approaches to suppress the current leakage in proton conducting oxides. Meanwhile, rationally controlling the chemical composition of proton conducting electrolyte is significant for the reduction of current leakage. To minimize the current leakage and improve the faradaic efficiency of electrolysis in H-SOECs, more efforts will be critically needed in the future.

The development of H-SOECs is still in the laboratory exploratory stage. To date, the largest H-SOECs reported in literature are tubular H-SOECs with air electrode area of 10 cm^2. Scaling up the footprint of the cells and demonstrating multi-cell stacks will be needed to demonstrate the advantages of H-SOECs in the future.

Acknowledgements

This work was primarily supported by National Key R&D Program of China (2017YFA0700104) and the US National Science Foundation (DMR–1832809).

M. N. acknowledges the funding support from Research Grant Council, University Grants Committee, Hong Kong SAR (Project Number: PolyU 152214/17E).

Received: ((will be filled in by the editorial staff))
Revised: ((will be filled in by the editorial staff))
Published online: ((will be filled in by the editorial staff))

Conflicts of interest

There are no conflicts to declare.

References

[1] L. Bi, S. Boulfrad, E. Traversa, *Chemical Society Reviews* **2014**, 43, 8255.

[2] S. H. Jensen, C. Graves, M. Mogensen, C. Wendel, R. Braun, G. Hughes, Z. Gao, S. A. Barnett, *Energy & Environmental Science* **2015**, 8, 2471.

[3] S. D. Ebbesen, S. H. Jensen, A. Hauch, M. B. Mogensen, *Chemical reviews* **2014**, 114, 10697.

[4] Y. Wang, T. Liu, L. Lei, F. Chen, *Fuel Processing Technology* **2017**, 161, 248.

[5] a) R. Xing, Y. Wang, Y. Zhu, S. Liu, C. Jin, *Journal of Power Sources* **2015**, 274, 260; b) Y. Li, Y. Li, Y. Wan, Y. Xie, J. Zhu, H. Pan, X. Zheng, C. Xia, *Advanced Energy Materials* **2018**, 1803156.

[6] a) M. Ni, M. K. Leung, D. Y. Leung, *Energy Conversion and Management* **2007**, 48, 1525; b) Y. Luo, Y. Shi, W. Li, N. Cai, *Energy* **2014**, 70, 420; c) H. Xu, B. Chen, M. Ni, *Journal of The Electrochemical Society* **2016**, 163, F3029.

[7] Y. Zheng, Q. Li, T. Chen, W. Wu, C. Xu, W. G. Wang, *International Journal of Hydrogen Energy* **2015**, 40, 2460.

[8] E. Vøllestad, R. Strandbakke, M. Tarach, D. Catalán-Martínez, M.-L. Fontaine, D. Beeaff, D. R. Clark, J. M. Serra, T. Norby, *Nature materials* **2019**, 1.

[9] E. Fabbri, D. Pergolesi, E. Traversa, *Chemical Society Reviews* **2010**, 39, 4355.

[10] Y. Zhang, R. Knibbe, J. Sunarso, Y. Zhong, W. Zhou, Z. Shao, Z. Zhu, *Advanced Materials* **2017**, 29.

[11] Z. Yang, M. Guo, N. Wang, C. Ma, J. Wang, M. Han, *International Journal of Hydrogen Energy* **2017**, 42, 24948.

[12] S. P. Jiang, X. Chen, *International Journal of Hydrogen Energy* **2014**, 39, 505.

[13] a) X. Yang, J. T. Irvine, *Journal of Materials Chemistry* **2008**, 18, 2349; b) T. Matsui, R. Kishida, J.-Y. Kim, H. Muroyama, K. Eguchi, *Journal of The Electrochemical Society* **2010**, 157, B776.

[14] M. Keane, M. K. Mahapatra, A. Verma, P. Singh, *International Journal of Hydrogen Energy* **2012**, 37, 16776.

[15] a) H. Iwahara, T. Esaka, H. Uchida, N. Maeda, *Solid State Ionics* **1981**, 3, 359; b) H. Iwahara, H. Uchida, N. Maeda, *Journal of Power Sources* **1982**, 7, 293.

[16] H. Iwahara, H. Uchida, I. Yamasaki, *International Journal of Hydrogen Energy* **1987**, 12, 73.

[17] a) H. Iwahara, T. Esaka, H. Uchida, T. Yamauchi, K. Ogaki, *Solid State Ionics* **1986**, 18, 1003; b) H. Iwahara, *Solid State Ionics* **1992**, 52, 99.

[18] P. A. Stuart, T. Unno, J. A. Kilner, S. J. Skinner, *Solid State Ionics* **2008**, 179, 1120.

[19] T. Sakai, S. Matsushita, H. Matsumoto, S. Okada, S. Hashimoto, T. Ishihara, *International Journal of Hydrogen Energy* **2009**, 34, 56.

[20] F. He, D. Song, R. Peng, G. Meng, S. Yang, *Journal of Power Sources* **2010**, 195, 3359.

[21] W. Wang, D. Medvedev, Z. Shao, *Advanced Functional Materials* **2018**, DOI: 10.1002/adfm.2018025921802592.

[22] a) K. D. Kreuer, *Annual Review of Materials Research* **2003**, 33, 333; b) T. Hibino, K. Mizutani, T. Yajima, H. Iwahara, *Solid State Ionics* **1992**, 57, 303.

[23] a) Z. Tao, L. Yan, J. Qiao, B. Wang, L. Zhang, J. Zhang, *Progress in Materials Science* **2015**, 74, 1; b) D. A. Medvedev, J. G. Lyagaeva, E. V. Gorbova, A. K. Demin, P.

Tsiakaras, *Progress in Materials Science* **2016**, 75, 38; c) H. Dai, H. Kou, H. Wang, L. Bi, *Electrochemistry Communications* **2018**, 96, 11.

[24] C. W. Tanner, A. V. Virkar, *Journal of The Electrochemical Society* **1996**, 143, 1386.

[25] S. V. Bhide, A. V. Virkar, *Journal of The Electrochemical Society* **1999**, 146, 2038.

[26] L. Bi, S. P. Shafi, E. Traversa, *Journal of Materials Chemistry A* **2015**, 3, 5815.

[27] a) J. Tong, D. Clark, L. Bernau, M. Sanders, R. O'Hayre, *Journal of Materials Chemistry* **2010**, 20, 6333; b) W. Sun, L. Yan, Z. Shi, Z. Zhu, W. Liu, *Journal of Power Sources* **2010**, 195, 4727; c) S. Ricote, N. Bonanos, A. Manerbino, N. P. Sullivan, W. G. Coors, *Journal of Materials Chemistry A* **2014**, 2, 16107.

[28] a) Y. Gan, J. Zhang, Y. Li, S. Li, K. Xie, J. T. S. Irvine, *Journal of the Electrochemical Society* **2012**, 159, F763; b) M. A. Azimova, S. McIntosh, *Solid State Ionics* **2011**, 203, 57; c) Y. Rao, S. Zhong, F. He, Z. Wang, R. Peng, Y. Lu, *International Journal of Hydrogen Energy* **2012**, 37, 12522; d) S. Li, K. Xie, *Journal of the Electrochemical Society* **2013**, 160, F224; e) Y. Yoo, N. Lim, *Journal of Power Sources* **2013**, 229, 48; f) C. Zuo, S. Zha, M. Liu, M. Hatano, M. Uchiyama, *Advanced Materials* **2006**, 18, 3318; g) Y. Guo, Y. Lin, R. Ran, Z. Shao, *Journal of Power Sources* **2009**, 193, 400.

[29] D. Huan, W. Wang, Y. Xie, N. Shi, Y. Wan, C. Xia, R. Peng, Y. Lu, *Journal of Materials Chemistry A* **2018**, 6, 18508.

[30] M. Hakim, C.-Y. Yoo, J. H. Joo, J. H. Yu, *Journal of Power Sources* **2015**, 278, 320.

[31] S. Yang, Y. Wen, S. Zhang, S. Gu, Z. Wen, X. Ye, *International Journal of Hydrogen Energy* **2017**, 42, 28549.

[32] L. Yang, S. Wang, K. Blinn, M. Liu, Z. Liu, Z. Cheng, M. Liu, *Science* **2009**, 326, 126.

[33] a) J. Kim, A. Jun, O. Gwon, S. Yoo, M. Liu, J. Shin, T.-H. Lim, G. Kim, *Nano Energy* **2018**, 44, 121; b) W. Wu, H. Ding, Y. Zhang, Y. Ding, P. Katiyar, P. K. Majumdar, T. He, D. Ding, *Advanced Science* **2018**, 1800360; c) S. Yang, S. Zhang, C. Sun, X. Ye, Z. Wen, *ACS Applied Materials&Interfaces* **2018**, 10, 42387.

[34] C. Duan, R. Kee, H. Zhu, N. Sullivan, L. Zhu, L. Bian, D. Jennings, R. O'Hayre, *Nature Energy* **2019**, 4, 230.

[35] a) C. Duan, J. Tong, M. Shang, S. Nikodemski, M. Sanders, S. Ricote, A. Almansoori, R. O'Hayre, *Science* **2015**, 349, 1321; b) S. Fang, K. S. Brinkman, F. Chen, *Journal of Membrane Science* **2014**, 467, 85; c) B. Hua, N. Yan, M. Li, Y. F. Sun, Y. Q. Zhang, J. Li, T. Etsell, P. Sarkar, J. L. Luo, *Advanced Materials* **2016**, 28, 8922.

[36] W. Li, B. Guan, L. Ma, H. Tian, X. Liu, *ACS Appl Mater Interfaces* **2019**, 11, 18323.

[37] a) C. Duan, R. J. Kee, H. Zhu, C. Karakaya, Y. Chen, S. Ricote, A. Jarry, E. J. Crumlin, D. Hook, R. Braun, N. P. Sullivan, R. O'Hayre, *Nature* **2018**, 557, 217; b) L. Lei, J. M. Keels, Z. Tao, J. Zhang, F. Chen, *Applied Energy* **2018**, 224, 280.

[38] a) Z. Sun, E. Fabbri, L. Bi, E. Traversa, *Physical chemistry chemical physics : PCCP* **2011**, 13, 7692; b) C.-Y. Yoo, D. S. Yun, J. H. Joo, J. H. Yu, *Journal of Alloys and Compounds* **2015**, 621, 263; c) S. W. Tao, J. T. S. Irvine, *Advanced Materials* **2006**, 18, 1581; d) S. Hossain, A. M. Abdalla, N. Radenahmad, A. K. M. Zakaria, J. H. Zaini, S. M. H. Rahman, S. G. Eriksson, J. T. S. Irvine, A. K. Azad, *International Journal of Hydrogen Energy* **2018**, 43, 894; e) Z. Liu, X. Wang, M. Liu, J. Liu, *International Journal of Hydrogen Energy* **2018**, 43, 13501; f) Y. Liu, Y. Guo, R. Ran, Z. Shao, *Journal of Membrane Science* **2013**, 437, 189.

[39] D. Han, S. Uemura, C. Hiraiwa, M. Majima, T. Uda, *ChemSusChem* **2018**, 11, 4102.

[40] a) W. Sun, Z. Shi, M. Liu, L. Bi, W. Liu, *Advanced Functional Materials* **2014**, 24, 5695; b) W. Sun, M. Liu, W. Liu, *Advanced Energy Materials* **2013**, 3, 1041; c) Y. Liu, Y. Guo, R. Ran, Z. Shao, *Journal of Membrane Science* **2012**, 415-416, 391; d) E. Fabbri, L. Bi, H. Tanaka, D. Pergolesi, E. Traversa, *Advanced Functional Materials* **2011**, 21, 158.

[41] D. Pergolesi, E. Fabbri, A. D'Epifanio, E. Di Bartolomeo, A. Tebano, S. Sanna, S. Licoccia, G. Balestrino, E. Traversa, *Nature Materials* **2010**, 9, 846.

[42] a) L. Bi, E. Fabbri, Z. Sun, E. Traversa, *Energy & Environmental Science* **2011**, 4, 409; b) S. Wang, Y. Liu, J. He, F. Chen, K. S. Brinkman, *International Journal of Hydrogen Energy* **2015**, 40, 5707.

[43] X. Xu, L. Bi, X. S. Zhao, *Journal of Membrane Science* **2018**, 558, 17.

[44] L. Lei, Z. Tao, X. Wang, J. P. Lemmon, F. Chen, *Journal of Materials Chemistry A* **2017**, 5, 22945.

[45] N. Shi, Y. Xie, D. Huan, Y. Yang, S. Xue, Z. Qi, Y. Pan, R. Peng, C. Xia, Y. Lu, *Journal of Materials Chemistry A* **2019**, 7, 4855.

[46] X.-F. Ye, Y. B. Wen, S. J. Yang, Y. Lu, W. H. Luo, Z. Y. Wen, J. B. Meng, *International Journal of Hydrogen Energy* **2017**, 42, 23189.

[47] a) N. Kochetova, I. Animitsa, D. Medvedev, A. Demin, P. Tsiakaras, *RSC Advances* **2016**, 6, 73222; b) Y. Wu, Z. Gong, J. Hou, L. Miao, H. Tang, W. Liu, *International Journal of Hydrogen Energy* **2019**, 44, 13835.

[48] R. Wang, M. Würth, U. B. Pal, S. Gopalan, S. N. Basu, *Journal of Power Sources* **2017**, 360, 87.

[49] Y. Niu, W. Lv, D. Chen, J. Han, W. He, *International Journal of Hydrogen Energy* **2019**, DOI: 10.1016/j.ijhydene.2019.05.115.

[50] L. Zhao, D. Ding, L. Zhang, L. Gui, Z. Wang, Y. Wan, R. Wang, Y. Ling, B. He, *International Journal of Hydrogen Energy* **2014**, 39, 18379.

[51] Y. Zhao, J. W. Fergus, *Journal of The Electrochemical Society* **2012**, 159, C109.

[52] P. Alnegren, M. Sattari, J.-E. Svensson, J. Froitzheim, *Journal of Power Sources* **2016**, 301, 170.

[53] R. Jacobs, T. Mayeshiba, J. Booske, D. Morgan, *Advanced Energy Materials* **2018**, 8, 1702708.

[54] Y. Chen, W. Zhou, D. Ding, M. Liu, F. Ciucci, M. Tade, Z. Shao, *Advanced Energy Materials* **2015**, 5, 1500537.

[55] Z. Zhao, L. Liu, X. Zhang, W. Wu, B. Tu, D. Cui, D. Ou, M. Cheng, *International Journal of Hydrogen Energy* **2013**, 38, 15361.

[56] N. Bausá, C. Solís, R. Strandbakke, J. M. Serra, *Solid State Ionics* **2017**, 306, 62.

[57] D. Huan, N. Shi, L. Zhang, W. Tan, Y. Xie, W. Wang, C. Xia, R. Peng, Y. Lu, *ACS Appl Mater Interfaces* **2018**, 10, 1761.

[58] S. Yang, Y. Wen, J. Zhang, Y. Lu, X. Ye, Z. Wen, *Electrochimica Acta* **2018**, 267, 269.

[59] J. Lyagaeva, N. Danilov, G. Vdovin, J. Bu, D. Medvedev, A. Demin, P. Tsiakaras, *Journal of Materials Chemistry A* **2016**, 4, 15390.

[60] N. Danilov, J. Lyagaeva, G. Vdovin, E. Pikalova, D. Medvedev, *Energy Conversion and Management* **2018**, 172, 129.

[61] W. Li, B. Guan, L. Ma, S. Hu, N. Zhang, X. Liu, *Journal of Materials Chemistry A* **2018**, 6, 18057.

[62] A. Grimaud, F. Mauvy, J. Marc Bassat, S. Fourcade, M. Marrony, J. Claude Grenier, *Journal of Materials Chemistry* **2012**, 22, 16017.

[63] R. Strandbakke, V. A. Cherepanov, A. Y. Zuev, D. S. Tsvetkov, C. Argirusis, G. Sourkouni, S. Prünte, T. Norby, *Solid State Ionics* **2015**, 278, 120.

[64] R. Zohourian, R. Merkle, G. Raimondi, J. Maier, *Advanced Functional Materials* **2018**, 28, 1801241.

[65] S. Choi, T. C. Davenport, S. M. Haile, *Energy & Environmental Science* **2019**, 12, 206.

[66] a) D. Ding, X. Li, S. Y. Lai, K. Gerdes, M. Liu, *Energy & Environmental Science* **2014**, 7, 552; b) H. J. Choi, K. Bae, S. Grieshammer, G. D. Han, S. W. Park, J. W. Kim, D. Y. Jang, J. Koo, J.-W. Son, M. Martin, J. H. Shim, *Advanced Energy Materials* **2018**, 8, 1802506; c) H. G. Seo, Y. Choi, W. Jung, *Advanced Energy Materials* **2018**, 8, 1703647.

[67] a) L. Lei, Z. Tao, T. Hong, X. Wang, F. Chen, *Journal of Power Sources* **2018**, 389, 1; b) G. Li, H. Jin, Y. Cui, L. Gui, B. He, L. Zhao, *Journal of Power Sources* **2017**, 341, 192; c) Y. Chen, S. Yoo, K. Pei, D. Chen, L. Zhang, B. deGlee, R. Murphy, B. Zhao, Y.

Zhang, Y. Chen, M. Liu, *Advanced Functional Materials* **2017**, DOI: 10.1002/adfm.2017049071704907.

[68] M. C. Tucker, *Journal of Power Sources* **2010**, 195, 4570.

[69] a) R. Wang, C. Byrne, M. C. Tucker, *Solid State Ionics* **2019**, 332, 25; b) R. Wang, G. Y. Lau, D. Ding, T. Zhu, M. C. Tucker, *International Journal of Hydrogen Energy* **2019**, 44, 13768.

[70] a) L. Bi, E. Fabbri, Z. Sun, E. Traversa, *Energy & Environmental Science* **2011**, 4, 1352; b) L. Bi, E. H. Da'as, S. P. Shafi, *Electrochemistry Communications* **2017**, 80, 20.

[71] K. Leonard, Y. Okuyama, Y. Takamura, Y.-S. Lee, K. Miyazaki, M. E. Ivanova, W. A. Meulenberg, H. Matsumoto, *Journal of Materials Chemistry A* **2018**, 6, 19113.

[72] S. Yang, Y. Lu, Q. Wang, C. Sun, X. Ye, Z. Wen, *International Journal of Hydrogen Energy* **2018**, 43, 20050.

[73] a) K. Xie, Y. Zhang, G. Meng, J. T. S. Irvine, *J. Mater. Chem.* **2011**, 21, 195; b) G. Wu, K. Xie, Y. Wu, W. Yao, J. Zhou, *Journal of Power Sources* **2013**, 232, 187; c) N. Danilov, A. Tarutin, J. Lyagaeva, G. Vdovin, D. Medvedev, *Journal of Materials Chemistry A* **2018**, 6, 16341.

[74] C. S. Tu, R. R. Chien, V. H. Schmidt, S. C. Lee, C. C. Huang, C. L. Tsai, *Journal of Applied Physics* **2009**, 105, 103504.

[75] a) M. Ni, M. K. Leung, D. Y. Leung, *International Journal of Hydrogen Energy* **2008**, 33, 4040; b) M. Ni, M. K. H. Leung, D. Y. C. Leung, *Journal of Power Sources* **2008**, 177, 369.

[76] L. Namwong, S. Authayanun, D. Saebea, Y. Patcharavorachot, A. Arpornwichanop, *Journal of Power Sources* **2016**, 331, 515.

[77] a) A. Grimaud, J. M. Bassat, F. Mauvy, P. Simon, A. Canizares, B. Rousseau, M. Marrony, J. C. Grenier, *Solid State Ionics* **2011**, 191, 24; b) D. Han, Y. Noda, T. Onishi,

N. Hatada, M. Majima, T. Uda, *International Journal of Hydrogen Energy* **2016**, 41, 14897.

[78] K.-Q. Zheng, M. Ni, Q. Sun, L.-Y. Shen, *Acta Mechanica Sinica* **2013**, 29, 388.

[79] D. P. Sutija, T. Norby, P. Björnbom, *Solid State Ionics* **1995**, 77, 167.

[80] M. Liu, H. Hu, *Journal of the Electrochemical Society* **1996**, 143, L109.

[81] a) J.-H. Zhang, L.-B. Lei, D. Liu, F.-Y. Zhao, M. Ni, F. Chen, *Journal of Power Sources* **2018**, 400, 333; b) S. Shen, Y. Yang, L. Guo, H. Liu, *Journal of Power Sources* **2014**, 256, 43.

[82] S. Shen, L. Guo, H. Liu, *International Journal of Hydrogen Energy* **2013**, 38, 1967.

[83] D. Poetzsch, R. Merkle, J. Maier, *Advanced Functional Materials* **2015**, 25, 1542.

[84] M. Liu, *Journal of the Electrochemical Society* **1997**, 144, 1813.

[85] a) H. Zhu, S. Ricote, C. Duan, R. P. O'Hayre, R. J. Kee, *Journal of The Electrochemical Society* **2018**, 165, F845; b) H. Zhu, S. Ricote, C. Duan, R. P. O'Hayre, D. S. Tsvetkov, R. J. Kee, *Journal of The Electrochemical Society* **2018**, 165, F581.

[86] A. V. Virkar, *Journal of Power Sources* **2009**, 194, 753.

[87] A. V. Virkar, *International Journal of Hydrogen Energy* **2012**, 37, 12609.

[88] M. Ni, D. Y. C. Leung, M. K. H. Leung, *Journal of Power Sources* **2008**, 183, 133.

[89] D. Poetzsch, R. Merkle, J. Maier, *Journal of Power Sources* **2013**, 242, 784.

[90] S. M. Babiniec, S. Ricote, N. P. Sullivan, *International Journal of Hydrogen Energy* **2015**, 40, 9278.

[91] G. Heras-Juaristi, D. Pérez-Coll, G. C. Mather, *Journal of Power Sources* **2017**, 364, 52.

[92] D. Han, T. Uda, *Journal of Materials Chemistry A* **2018**, 6, 18571.

[93] M. Dippon, S. M. Babiniec, H. Ding, S. Ricote, N. P. Sullivan, *Solid State Ionics* **2016**, 286, 117.

[94] a) T. Yajima, H. Iwahara, H. Uchida, *Solid State Ionics* **1991**, 47, 117; b) C. Zhang, H. Zhao, *Solid State Ionics* **2010**, 181, 1478.

[95] a) J. Cao, Z. Gong, J. Hou, J. Cao, W. Liu, *Ceramics International* **2015**, 41, 6824; b) Z. Wang, X. Huang, Z. Lv, Y. Zhang, B. Wei, X. Zhu, Z. Wang, Z. Liu, *Ceramics International* **2015**, 41, 4410; c) B. Shri Prakash, R. Pavitra, S. Senthil Kumar, S. T. Aruna, *Journal of Power Sources* **2018**, 381, 136.

[96] B. Zhang, Z. Zhong, T. Tu, K. Wu, K. Peng, *Journal of Power Sources* **2019**, 412, 631.

[97] T. Kobayashi, K. Kuroda, S. Jeong, H. Kwon, C. Zhu, H. Habazaki, Y. Aoki, *Journal of The Electrochemical Society* **2018**, 165, F342.

Figures and tables

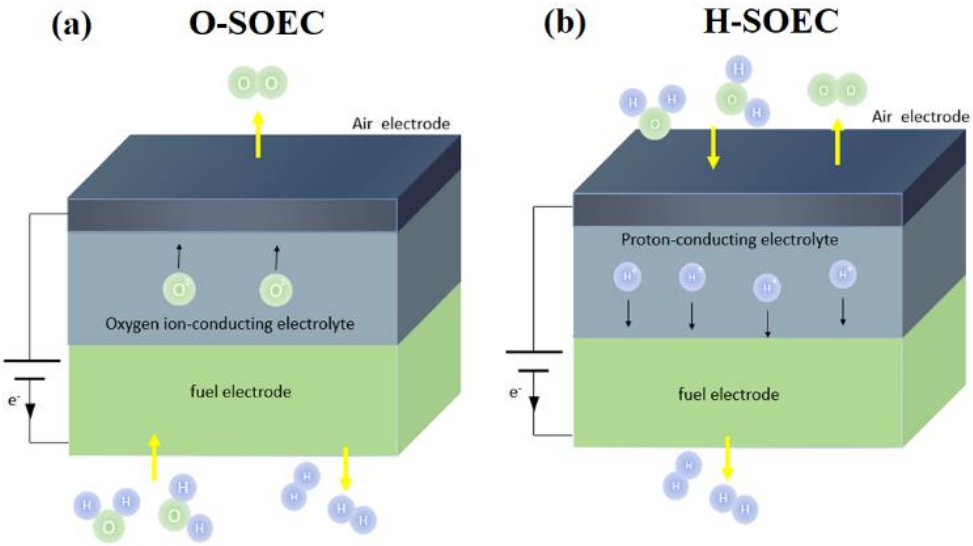

Figure 1 Schematics of two types of SOECs (a) O-SOEC; (b) H-SOEC.

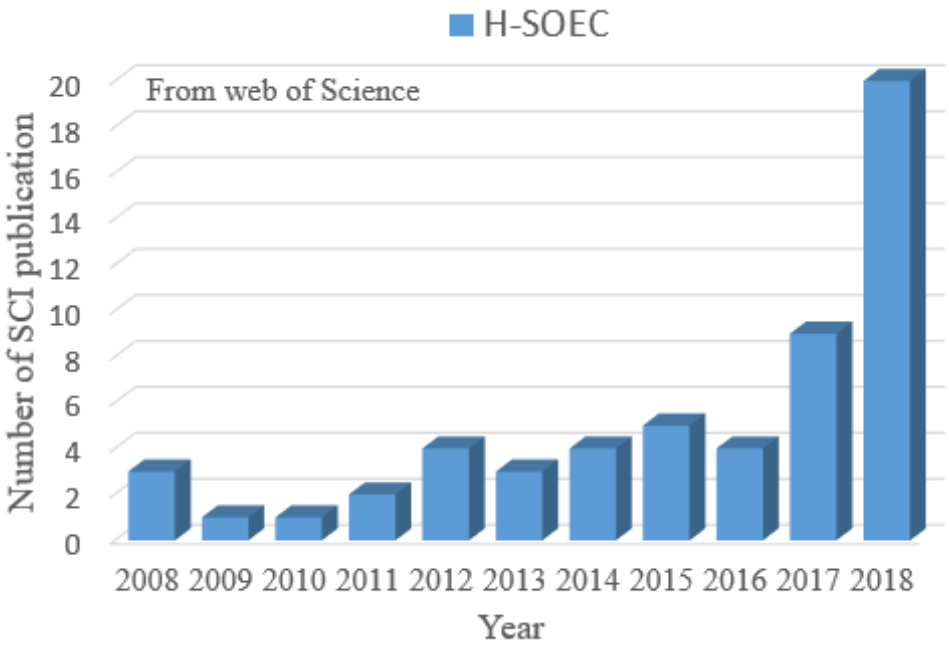

Figure 2 The number of SCI papers about H-SOECs from 2008 to 2018

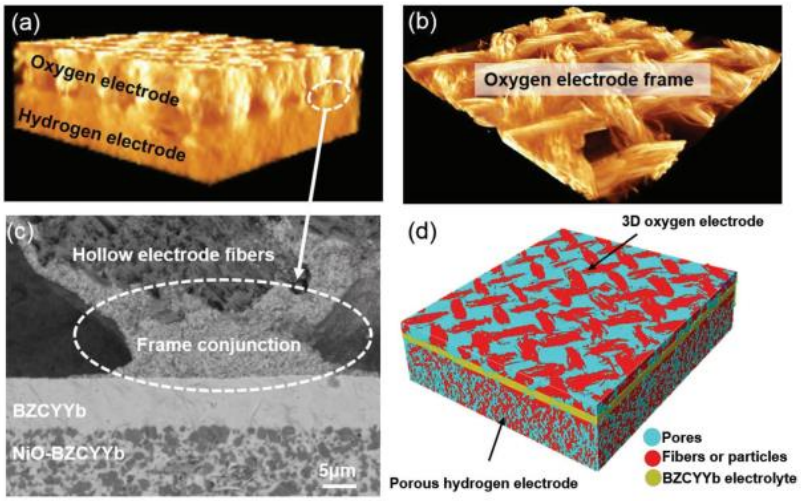

Figure 3 (a) 3D X-ray microscopic image for the cell consisting fuel electrode (bottom layer), electrolyte (invisible) and 3D air electrode (top layer); (b) The bulk electrode frame with hierarchical gaps; (c) SEM image for the cross section of the cells; (d)

reconstructed 3D image for the cell. Reproduced by permission.[33b] Copyright 2018, Wiley.

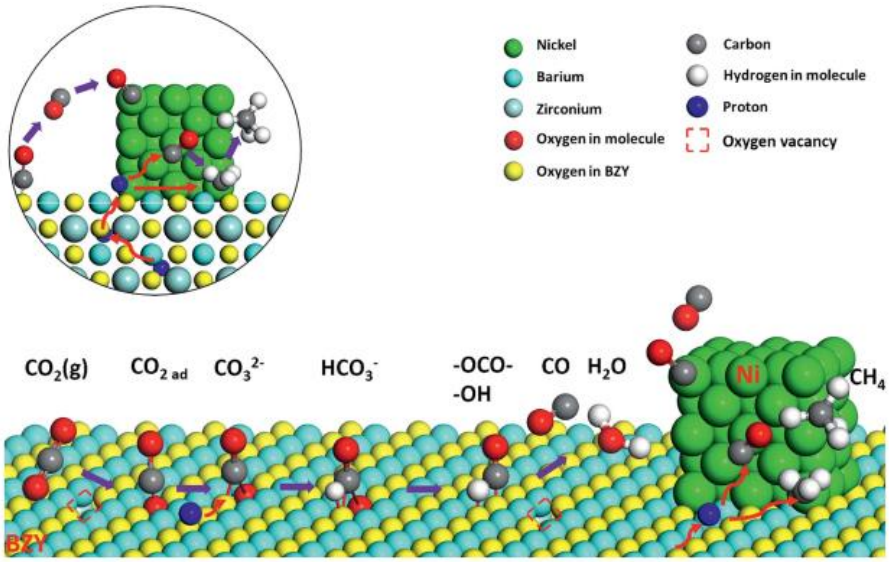

Figure 4 Schematic of possible reaction mechanism for CO_2 conversion in H-SOECs with applied electrolysis current. The atom radius and bond length in the diagram are not proportional and only shown for illustration. Reproduced by permission.[45] Copyright 2018, Royal Society of Chemistry.

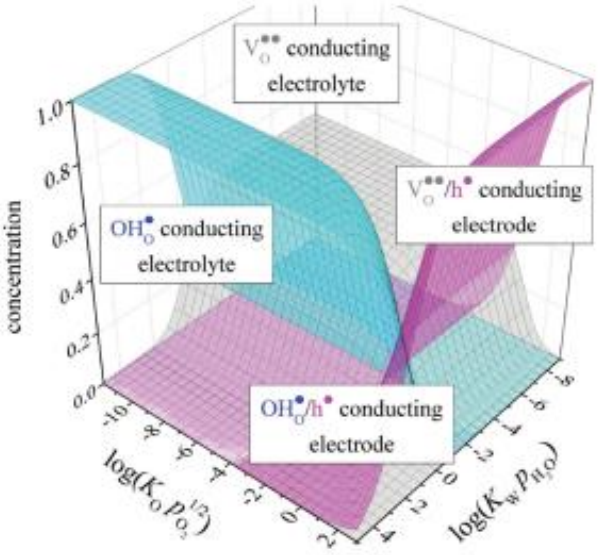

Figure 5 Concentrations of defects in an acceptor-doped oxide as functions of $K_W p_{H_2O}$ and $K_O p_{O_2}^{1/2}$. Reproduced by permission.[83] Copyright 2015, Wiley.

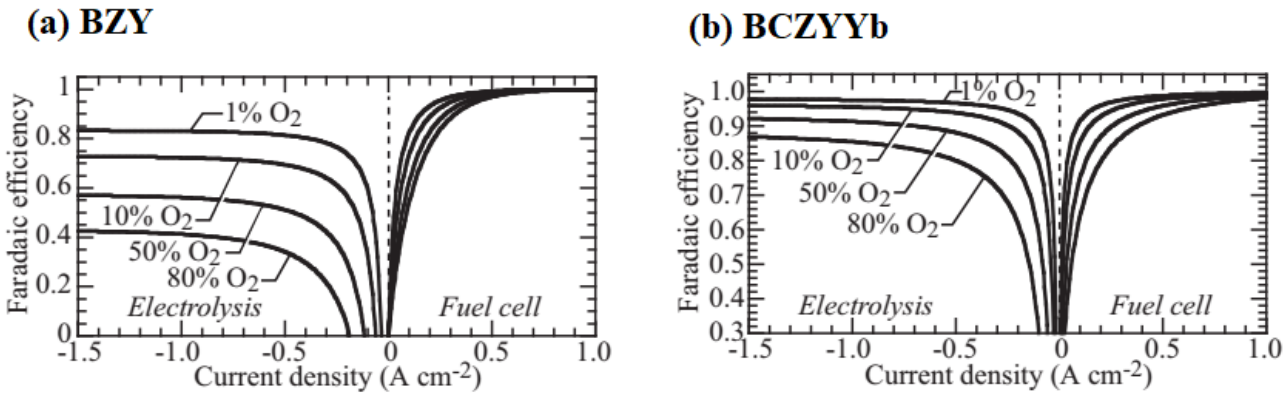

Figure 6 Faradic efficiency of proton-conducting cells in the fuel cell and electrolysis mode (a) BZY as electrolyte material; (b) BCZYYb as electrolyte material. Reproduced by permission. [85] Copyright 2018, The Electrochemical Society.

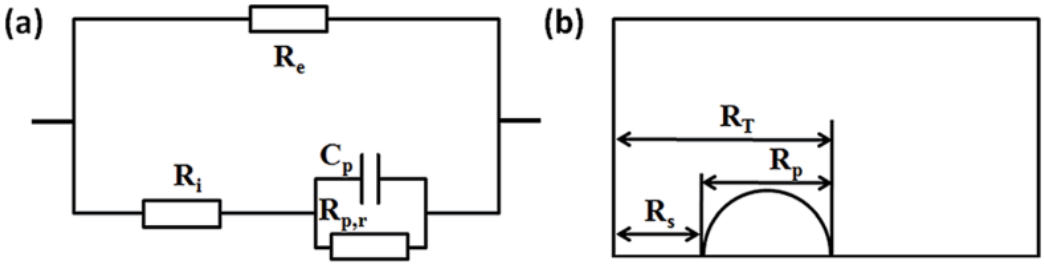

Figure 7 (a) An equivalent circuit for H-SOC; (b) Simulated impedance spectra for circuit (a). Reproduced by permission.[29] Copyright 2018, Royal Society of Chemistry.

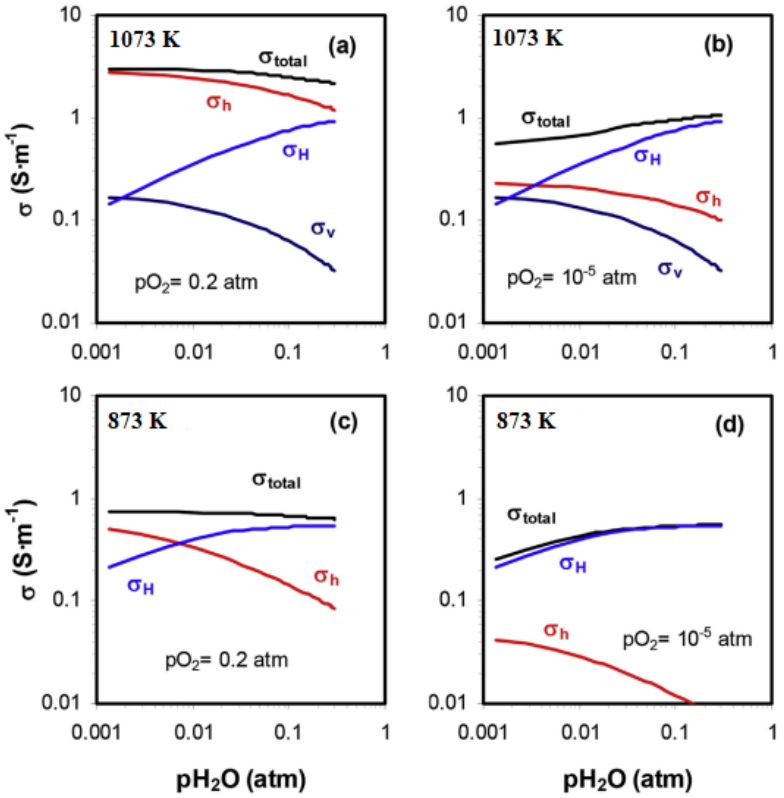

Figure 8 In BCZY27, the representation of the partial conductivity of oxygen ion, proton and electron hole as a function of pH_2O (a) at 1073 K and pO_2=0.2atm; (b) at 1073 K and pO_2=10^{-5}atm; (c) at 873 K and pO_2=0.2atm; (d) at 873 K and pO_2=10^{-5}atm. Reproduced by permission.[91] Copyright 2017, Elsevier.

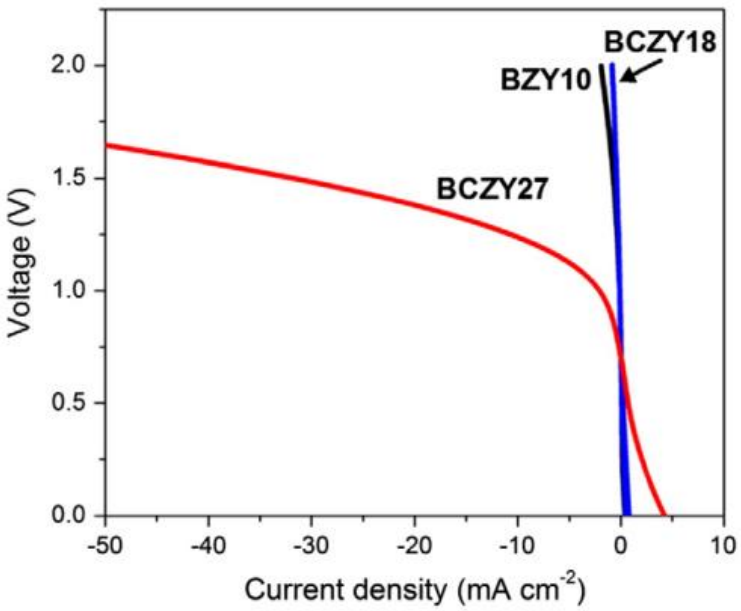

Figure 9 Comparison of the polarization characteristics for the BZY10, BCZY18 and BCZY27 membranes at 923 K. Dry 10% He-90% Ar at Au electrode and dry 10% H_2-90% Ar at Ni-BCZY27 electrode. Reproduced by permission.[93] Copyright 2016, Elsevier.

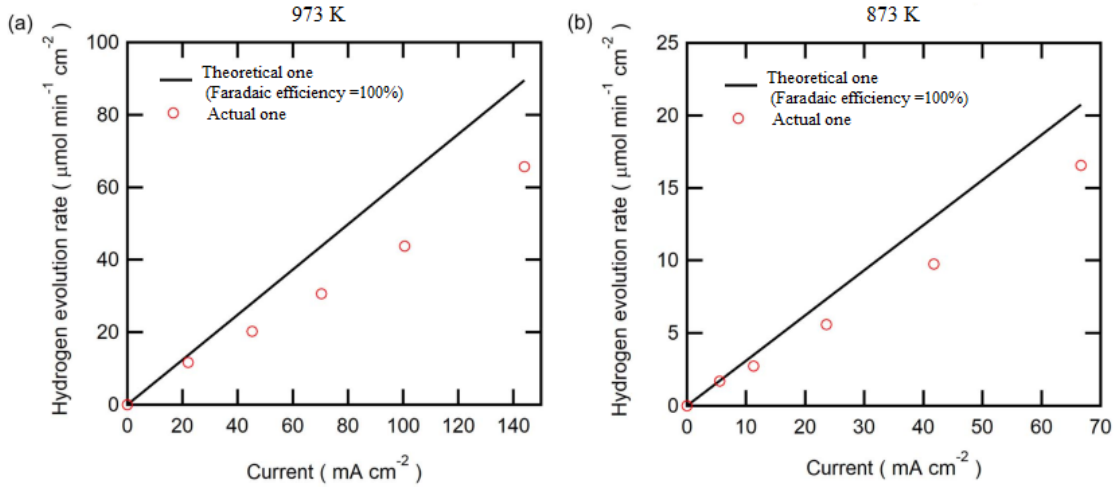

Figure 10 Hydrogen evolution rate in H-SOECs with BCZY44 as electrolyte (a) at 973 K; (b) at 873 K. Reproduced by permission.[97] Copyright 2018, The Electrochemical Society.

Table 1 Comparison of the performance of H-SOECs at 1.3 V

Configuration of electrolysis cell	Operation temperature (K)	Inlet gas composition in the air electrode	Absolute current density (mA cm^{-2})	[Ref.] year
Pt/BCY10(450 μm)/Pt	873	air	12	[18] 2008
SSC-BCZY/BCZY53 (20 μm)/Ni-BCZY53	873	50% H_2O,50% Air	~190	[20] 2010
LSC-BCZYbCo/BCZYbCo (45 μm)/Ni-BCZYbCo	873	3% H_2O,19.4% O_2, 77.6% He	16	[28b] 2011
LSCM-BZCYZ53/BZCYZ53(75 μm)/Ni-BCZY53	973	3% H_2O, 97% N_2	960	[28a] 2012
BZCo /BCZY53 (20 μm)/Ni-BCZY53	973	30% H_2O, 70% Air	460	[28c] 2012
LSCF- BCZYZ53/BCZYZ53 (2000 μm)/Ni-BCZYZ53	1073	3% H_2O, 97% Air	26	[28d] 2013
BSCF-BCZY62 /BCZY62 (15 μm)/BCZY62-Ni	873	3% H_2O, 97% Air	~1000	[28e] 2013
LSCF-BZY/BZY20 (15 μm)/Ni-BZY20	873	3% H_2O, 97% Air	53	[26] 2015
LNF/LN-BCZD53/BCZD53 (30 μm)/Ni-BCZD53	873	90% H_2O, 10% Air	~170	[59] 2016
SFM-BZY/BZY20 (16 μm)/Ni-BZY20	873	3% H_2O, 97% Air	210	[44] 2017
LSM/BCZI3(15 μm)/ Ni-BCZI3	873	20% H_2O, 80% Air	~120	[31] 2017
LSC-CZI/CZI (15 μm)/ Ni-CZI3	1073	20% H_2O, 80% Air	~200	[46] 2017
NBN/BCZD53 (15 μm)/Ni- BCZD53	873	30% H_2O, 70% Air	~200	[60] 2018
SEFC/BCZY71 (15 μm)/BCZY71-Ni	873	10% H_2O, 90% Air	~350	[57] 2018
SLF/BCZY53 (20 μm)/BCZY53-Ni	873	20% H_2O, 80% Air	460	[29] 2018
NBSCF-BCZYYb/BCZYYb (20 μm)/BCZYYb-Ni	873	10% H_2O, 90% Air	750	[33a] 2018
PNO-BCZY62/ BCZY62 (15 μm)/Ni- BCZY62	873	40% H_2O, 60% Air	600	[61] 2018
PSN/BCZY71 (15 μm)/ Ni- BCZY71(active layer)/Ni- BCZY71	873	20% H_2O, 80% Air	350	[58] 2018
LSN/BCZY71 (16 μm)/ Ni- BCZY71(active layer) /Ni- BCZY71	873	20% H_2O, 80% Air	420	[72] 2018
PBSCF(3D)/BCZYYb (20 μm)/BCZYYb-Ni	873	12% H_2O, 88% Air	850	[33b] 2018
LSN- BCZYYC2/ BCZYYC2(13μm)/ Ni- BCZYYC2(active layer)/Ni-BCZYYC2	873	20% H_2O, 80% Air	600	[33c]2018

Configuration of electrolysis cell	Operation temperature (K)	Inlet gas composition in the air electrode	Absolute current density (mA cm^{-2})	[Ref.] year
BLC/BCZY(45)$_{8/9}$2 (12 µm)/SCZY451-Ni	873	80% H_2O, 1% O_2	~250	[71] 2018
PBSCF(PLD-modified)/BCZYYb4411 (15 µm)/ BCZYYb4411-Ni	873	3% H_2O, 97% Air	~2000	[65] 2019
SEFC/BZY20 (15 µm)/BZY20-Ni	873	10% H_2O, 90% Air	760	[45] 2019
BCFZY/BCZYYb (12 µm)/BCZYYb-Ni	873	10% H_2O, 90% Air	~1100	[34] 2019
PNO/LCO/BCZYYb(20 µm)/BCZYYb-Ni	873	60% H_2O, 40% Air	330	[36] 2019
BGLC-BCZY27(10 cm^2)/BCZY27/BCZY-Ni (tubular)	873	50% H_2O, 0.03% O_2, 47.3% Ar (3 bar)	~80	[8] 2019

For electrolyte

BCY10= $BaCe_{0.9}Y_{0.1}O_{3-\delta}$; BCZY53= $BaCe_{0.5}Zr_{0.3}Y_{0.2}O_{3-\delta}$; BCZYbCo=$BaCe_{0.48}Zr_{0.4}Yb_{0.1}Co_{0.02}O_{3-\delta}$; BCZYZ53= $BaCe_{0.5}Zr_{0.3}Y_{0.16}Zn_{0.04}O_{3-\delta}$; BCZY62= $BaCe_{0.6}Zr_{0.2}Yb_{0.2}O_{3-\delta}$; BCZD53=$BaCe_{0.5}Zr_{0.3}Dy_{0.2}O_{3-\delta}$; BCZI523= $BaCe_{0.5}Zr_{0.2}In_{0.3}O_{3-\delta}$; CZI=$CaZr_{0.9}In_{0.1}O_{3-\delta}$; BZY20= $BaZr_{0.8}Y_{0.2}O_{3-\delta}$; BCZY71= $BaCe_{0.7}Zr_{0.1}Yb_{0.2}O_{3-\delta}$; BCZY27= $BaCe_{0.2}Zr_{0.7}Yb_{0.1}O_{3-\delta}$; BCZYYb=$BaCe_{0.7}Zr_{0.1}Y_{0.1}Yb_{0.1}O_{3-\delta}$; BCZYYC2=$BaCe_{0.68}Zr_{0.1}Y_{0.1}Yb_{0.1}Cu_{0.02}O_{3-\delta}$; BCZYYb4411=$BaCe_{0.4}Zr_{0.4}Y_{0.1}Yb_{0.1}O_{3-\delta}$; BCZY(45)$_{8/9}$2= $Ba(Ce_{0.4}Zr_{0.5})_{8/9}Y_{0.2}O_{3-\delta}$; SZCY541= $SrCe_{0.4}Zr_{0.5}Y_{0.1}O_{3-\delta}$, LCO= $La_2Ce_2O_7$.

For air electrode

SSC= $Sr_{0.5}Sm_{0.5}CoO_3$;BZCo= $BaZr_{0.6}Co_{0.4}O_{3-\delta}$; LSCM= $(La_{0.75}Sr_{0.25})_{0.95}Mn_{0.5}Co_{0.5}O_{3-\delta}$; BSCF= $Ba_{0.50}Sr_{0.50}Co_{0.80}Fe_{0.20}O_{3-\delta}$; LSM=$(La_{0.8}Sr_{0.2})_{0.98}MnO_3$; LNF= $La_2Ni_{0.6}Fe_{0.4}O_{3-\delta}$; LN= $La_2NiO_{4+\delta}$; SFM= $Sr_2Fe_{1.5}Mo_{0.5}O_6$; LSC=$La_{0.6}Sr_{0.4}CoO_3$; NBN=$Nd_{1.95}Ba_{0.05}NiO_{4+\delta}$; SEFC= $SrEu_2Fe_{1.8}Co_{0.2}O_{7-\delta}$; SLF= $Sr_{2.8}La_{0.2}Fe_2O_{7-\delta}$; NBSCF= $NdBa_{0.5}Sr_{0.5}Co_{1.5}Fe_{0.5}O_{5+\delta}$; PNO= $Pr_2NiO_{4+\delta}$; LSN= $La_{1.2}Sr_{0.8}NiO_4$; PSN=$Pr_{1.2}Sr_{0.8}NiO_4$; PBSCF= $PrBa_{0.5}Sr_{0.5}Co_{2-x}Fe_xO_{5+\delta}$; BLC= $Ba_{0.5}La_{0.5}CoO_{3-\delta}$; BCFZY=$BaCo_{0.4}Fe_{0.4}Zr_{0.1}Y_{0.1}O_{3-\delta}$; BGLC=$Ba_{0.5}Gd_{0.8}La_{0.7}Co_2O_{6-\delta}$.

Author biographies and photographs

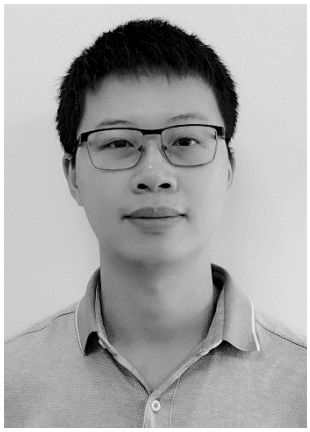

Libin Lei is currently an Associate Professor in the School of Materials and Energy in Guangdong University of Technology (GDUT). He received a Bachelor's Degree in Chemical Engineering (2010) from GDUT, a Master's Degree in Applied Chemistry (2013) from South China University of Technology, and a Ph.D in Mechanical Engineering (2018) from University of South Carolina. His current research focuses on the system design and materials development for electrochemical devices such as solid oxide cells.

Jihao Zhang is currently a post-doctoral fellow in Tsinghua University. He received his BS and PhD. degrees from China University of Petroleum in 2014 and Wuhan University in 2019, respectively. He joined University of South Carolina as a Joint PhD. student during 2017-2018. His research interests are electrochemical energy conversion and computational fluid dynamics, especially to study the internal short circuit of solid oxide fuel cells (SOFCs).

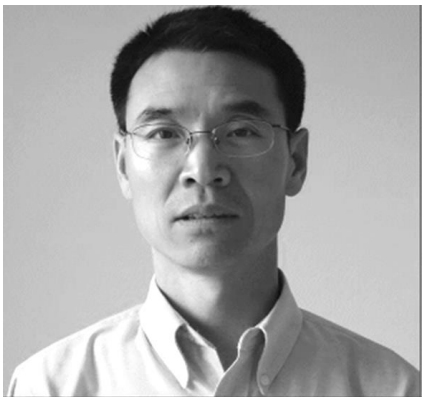

Fanglin (Frank) Chen is currently a Full Professor in the Department of Mechanical Engineering at University of South Carolina. He received a Bachelor's Degree in Chemistry from Anhui University, a Masters Degree in Materials Science and Engineering from University of Science and Technology of China, and a Ph.D in Materials Science and Engineering from Georgia Institute of Technology. His research interests are in the area of synthesis and characterization of novel materials for electrochemical and catalytic applications such as solid oxide fule cells, solid oxide electrolysis cell, and membrane reactors.